

---

# DiRecT: Safe Diffusion-Based Planning via Receding-Horizon Denoising

---

Paolo Giarretta  
MIT  
pgiarett@mit.edu

Zeyang Li  
MIT  
zeyang@mit.edu

Navid Azizan  
MIT  
azizan@mit.edu

## Abstract

Diffusion models have emerged as powerful tools for planning and control by learning multimodal distributions over actions and trajectories. Yet reliable inference-time safety enforcement remains a key barrier to their deployment in safety-critical tasks. Existing approaches typically project each denoising iterate onto the feasible set, even though constraints are defined only on the final clean trajectory. Enforcing feasibility on noisy intermediate samples can therefore overconstrain the sampling dynamics, substantially degrading sample quality. To address this limitation, we introduce DiRecT (**D**iffusion-based planning via **R**eceding-horizon denoising with **T**erminal constraints), a training-free algorithm for constrained sampling from diffusion models via stochastic optimal control (SOC). DiRecT enforces constraints only on the final clean sample, avoiding unnecessary restrictions on the intermediate denoising dynamics. Inspired by model predictive control, we derive a principled receding-horizon surrogate for the otherwise intractable constrained SOC formulation, yielding an efficient algorithm that cleanly separates stochastic denoising from constraint satisfaction, progressively steering samples toward feasible final trajectories without distorting the learned diffusion dynamics. Furthermore, DiRecT is highly flexible: it can leverage off-the-shelf or domain-specific optimizers, incorporate priors over environment dynamics, and optimize additional soft rewards. Extensive experiments on safe planning benchmarks demonstrate that DiRecT substantially improves deployment safety and task performance over existing diffusion-based planning baselines. Our code is available at <https://github.com/azizanlab/DiRecT>.

## 1 Introduction

Safe and reliable planning remains a central challenge, requiring algorithms that can satisfy constraints while adapting to diverse environments, objectives, and constraint types. Classical planning methods [25, 32, 33, 36, 51, 57] have achieved strong results in many structured settings, but they face important limitations. Search-based methods can become computationally prohibitive in large-scale multi-agent problems [70], while optimization-based methods are often local and sensitive to initialization [51, 57]. These limitations have driven growing interest in *data-driven* generative planners, which learn reusable priors from offline data and can model diverse, high-dimensional behaviors. Building on their success in image generation [17], diffusion models [28, 60, 62] have emerged as a powerful framework for planning and control, capable of capturing complex, multimodal state-action distributions [29] while supporting flexible inference-time guidance [1].

Despite these advances, deploying diffusion-based planners in real-world safety-critical tasks remains challenging. For instance, a generated trajectory must avoid collisions with obstacles, as even a single violation can lead to catastrophic failure. Since diffusion models rely on high-dimensional stochastic denoising dynamics, typically parameterized by large neural networks, they may generate

---

Correspondence to Zeyang Li (zeyang@mit.edu).

unsafe plans even when trained on feasible trajectories. This challenge is further amplified when trajectories must satisfy novel constraints that are not captured by the dataset. These limitations have motivated growing interest in *test-time* mechanisms for constraining diffusion planners. Inspired by guidance techniques in image generation [15, 17, 27], early approaches steer samples during denoising by encoding constraint satisfaction as a *soft* guidance signal [45]. However, soft guidance can only encourage feasibility and does not guarantee hard constraint satisfaction. More recent work has therefore focused on enforcing hard constraints directly on sampled trajectories, with the goal of providing stronger guarantees for safety-critical planning. Particularly, most hard-constrained diffusion samplers enforce feasibility through projections or constraint-driven updates along the denoising trajectory [14, 39, 43, 69, 71]. This creates a mismatch: planning constraints are defined on the final clean trajectory, while intermediate denoising iterates are noisy and need not themselves be feasible. Imposing constraints throughout sampling can therefore overconstrain the learned reverse dynamics, significantly degrading sample quality. Moreover, projection-based formulations do not naturally provide a unified mechanism for handling hard constraints together with additional soft rewards or costs.

To address these limitations, we introduce DiRecT (**D**iffusion-based planning via **R**eceding-horizon denoising with **T**erminal constraints), a *training-free* algorithm for constrained sampling in diffusion-based planning. We formulate inference-time constraint enforcement through the lens of stochastic optimal control (SOC) [31], where the learned reverse diffusion process serves as the nominal stochastic dynamics and control inputs steer the sampler toward feasibility of the final clean trajectory. Crucially, constraints are imposed only on this terminal clean sample, avoiding unnecessary restrictions on noisy intermediate denoising iterates.

Solving the resulting terminally constrained SOC problem is computationally intractable. We therefore exploit the structure of diffusion models, together with ideas from model predictive control (MPC) [52], to derive a principled and scalable receding-horizon surrogate. At each denoising step, DiRecT predicts the final clean trajectory implied by the current noisy iterate, solves a constrained optimization problem over this prediction, and converts the resulting refinement into a controlled update of the current noisy iterate.

The contributions of this paper are:

- We identify a key limitation of prior constrained diffusion samplers: enforcing feasibility on noisy intermediate denoising iterates can overconstrain the sampling dynamics and degrade sample quality. In contrast, we formulate training-free constrained diffusion planning as a terminally constrained SOC problem that enforces feasibility only on the final clean trajectory while staying close to the learned diffusion dynamics.
- We present DiRecT, a training-free constrained diffusion sampler that reduces the intractable constrained SOC problem to a sequence of tractable clean-trajectory optimization sub-problems. By refining predicted clean trajectories and translating these refinements into controlled updates of the noisy iterates, DiRecT steers samples toward constraint satisfaction without distorting the learned denoising process.
- We show that DiRecT is highly flexible, supporting off-the-shelf and domain-specific optimizers, equality and inequality constraints, environment-specific dynamics priors, and additional soft rewards or costs at inference time.
- We evaluate DiRecT across diverse robotic planning applications, including maze navigation in Maze2D, robotic manipulation in D3IL, multi-robot motion planning (MRMP), and diverse contact-rich manipulation in PushT. Across these tasks, DiRecT consistently improves constraint satisfaction and task success over existing diffusion-based planning baselines.

## 2 Related Work

This section situates our work within the broader literature. First, we review constrained sampling techniques for diffusion-based planners, emphasizing the key limitation that motivates our method. Second, we discuss prior work that also explores connections between diffusion models and stochastic optimal control, clarifying how our constrained sampling perspective differs from these approaches. Finally, we mention a parallel but complementary line of work on training-based methods for planning with diffusion models. Due to space constraints, the details are deferred to Appendix A.

### 3 Background

**Diffusion models.** We employ the continuous-time formulation and define diffusion models as a pair of Itô processes: a *forward* process that gradually corrupts samples drawn from the data distribution  $p_0$  through the stochastic differential equation (SDE)  $dX_t = f_t(X_t)dt + g_t(X_t)dW_t$ ,  $X_0 \sim p_0$ ,  $t \in [0, 1]$ , and a *backward* process that generates samples starting from the simple prior distribution  $p_1 \approx \mathcal{N}(0, I_d)$  by time reversal of the forward SDE [3]:

$$dX_t = [f_t(X_t) - g_t^2(X_t)\nabla_{X_t} \log p_t(X_t)] dt + g_t(X_t)d\bar{W}_t, \quad X_1 \sim p_1, \quad (1)$$

where (1) is integrated backward in time,  $W_t$  and  $\bar{W}_t$  denote the forward and backward Wiener processes, and  $s_t(x_t) = \nabla_{x_t} \log p_t(x_t)$  is the score function of the marginal distribution  $p_t$ . Moreover, we restrict our focus to the common case of Gaussian-affine schedules, for which the conditional distribution of the forward noising process has the closed-form solution  $q_t(x_t|x_0) = \mathcal{N}(\alpha_t x_0, \sigma_t^2 I_d)$ , where the noise-schedule coefficients  $\{\alpha_t, \sigma_t\}_{t \in [0,1]}$  are related to the SDE drift and diffusion functions by  $f(x, t) = \frac{\dot{\alpha}_t}{\alpha_t} x$ ,  $g^2(t) = \frac{d}{dt} \sigma_t^2 - 2 \frac{\dot{\alpha}_t}{\alpha_t} \sigma_t^2$ . Following denoising score matching [62, 67], the score function  $s_t(x_t)$  is approximated by a neural network  $s_t^\theta(x_t)$  trained to minimize the conditional score-matching (CSM) loss:

$$\mathcal{L}_{\text{CSM}}(\theta) = \mathbb{E}_{t, x_0, \varepsilon} \left[ \lambda(t) \left\| s_t^\theta(\alpha_t x_0 + \sigma_t \varepsilon) + \frac{\varepsilon}{\sigma_t} \right\|^2 \right], \quad (2)$$

where  $t \sim \mathcal{U}[0, 1]$ ,  $x_0 \sim p_0$ ,  $\varepsilon \sim \mathcal{N}(0, I_d)$ , and  $\lambda(t)$  is a time-dependent weighting.

**Sampling and Tweedie’s formula.** Sampling from a diffusion model is achieved by numerically simulating the reverse dynamics (1) using the learned score function. Common stochastic samplers include DDPM [28], Euler–Maruyama [35], and higher-order solvers [42]. Despite our focus on *stochastic* dynamics, few-step *deterministic* samplers are commonly obtained by numerical integration of the probability-flow ODE [62], which shares the same marginal distributions as (1). Examples include DDIM [61] and ODE-based solvers [41]. A one-step instantiation of these samplers yields an approximation of the posterior conditional mean of the forward process, which is related to the score function through Tweedie’s formula [54]:

$$\mathbb{E}[X_0 | X_t] \approx \hat{x}_0^\theta(x_t, t) = \frac{x_t + \sigma_t^2 s_t^\theta(x_t)}{\alpha_t}. \quad (3)$$

Therefore, we use  $s_t^\theta$  and  $\hat{x}_0^\theta$  interchangeably when convenient, assuming they are related by (3).

**Diffusion planners.** Following diffusion-based planning formulations [13, 29], we treat the clean sample as a finite-horizon plan rather than a single configuration. Let  $H \in \mathbb{N}$  be the prediction horizon and let  $\mathcal{H} = \{0, \dots, H\}$ . We denote plans as  $\tau = (\tau_0, \dots, \tau_H) \in \mathcal{D}^{H+1}$ , where each element  $\tau_k \in \mathcal{D} \subseteq \mathbb{R}^D$  may encode a state, an action, or a state-action pair depending on the planner parameterization. A diffusion planner learns a distribution over such plans and generates  $\tau$  by denoising a Gaussian prior sample. In closed-loop deployment, the planner executes only the first  $M \leq H$  elements before re-planning, and the concatenation of executed prefixes forms the rollout.

### 4 Method

We now formalize hard-constrained sampling for diffusion models and derive DiRecT. The derivation is similar in spirit to the test-time guidance framework for flow-matching models developed in [38], while differing in the diffusion-model setting and the resulting algorithmic form. Due to space limitations, we defer the full derivation of the algorithm to Appendix C. Given a pretrained score model, a constraint set  $\mathcal{S} \subseteq \mathbb{R}^d$ , and a cost function  $C : \mathbb{R}^d \rightarrow \mathbb{R}$ , we seek to sample denoised plans  $\tau$  from the model that are: (i) *safe* ( $\tau \in \mathcal{S}$ ), (ii) *minimize* the cost  $C$ , and (iii) remain *proximal* to the learned data distribution. We now expand on the problem setting and show how safe planning can naturally be framed as solving a stochastic optimal control problem with terminal constraints. We then derive a receding-horizon surrogate formulation that leads to a tractable algorithm. In this section, we use a general diffusion-centric notation and denote denoised plans as  $X_0$ .

**Safe planning with diffusion models and stochastic optimal control.** Denote by  $\tilde{f}_t^\theta(X_t)$  the reverse drift  $f_t(X_t) - g(t)^2 s_t^\theta(X_t)$ , so that the sampling dynamics of the trained model are  $dX_t = \tilde{f}_t^\theta(X_t)dt + g(t)d\bar{W}_t$ ,  $X_1 \sim p_1$ . Let  $u : \mathbb{R}^d \times [0, 1] \rightarrow \mathbb{R}^d$  be a control drift that steers the generative process toward low-cost feasible samples through the controlled SDE:

$$dX_t^u = \left[ \tilde{f}_t^\theta(X_t^u) + g(t)u_t(X_t^u) \right] dt + g(t)d\bar{W}_t, \quad X_1 \sim p_1 \quad (4)$$

Our three requirements for a safe, performant, and proximal planner naturally fit within a terminally constrained stochastic optimal control perspective [8], which aims to find the optimal control that solves Problem 1:

**Problem 1** (Stochastic optimal control problem with terminal constraints). *Given reference dynamics, constraint set  $\mathcal{S}$ , terminal cost  $C$ , and cost weight  $\lambda$ , solve for the optimal control drift  $u^*$ :*

$$\begin{aligned} \min_u \quad & \mathbb{E} \left[ \lambda C(X_0^u) + \frac{1}{2} \int_0^1 \|u_t(X_t^u)\|_2^2 dt \right] \\ \text{s.t.} \quad & dX_t^u = \left[ \tilde{f}_t^\theta(X_t^u) + g(t)u_t(X_t^u) \right] dt + g(t)d\bar{W}_t, \quad X_1 \sim p_1 \\ & X_0^u \in \mathcal{S} \quad \mathbb{P}^u\text{-a.s.} \end{aligned} \quad (5)$$

where  $\mathbb{P}^u$  denotes the path measure induced by (4). Notably, Problem 1 enforces constraint satisfaction only at the terminal state. Intermediate latents may therefore deviate significantly from the feasible set if doing so reduces control energy and keeps the process closer to the pretrained dynamics. In principle, the optimal controller can be obtained by solving the Hamilton–Jacobi–Bellman (HJB) [5] equation. However, exact solutions are rarely possible for the rich, high-dimensional dynamics induced by the backward SDE. See Appendix B for an overview of SOC, the HJB equation, and their relation to KL control.

**Receding-horizon surrogate formulation.** We briefly summarize the main steps used to transform the continuous-time SOC problem into a tractable receding-horizon surrogate. We first discretize the reverse dynamics in (1). Let  $N \in \mathbb{N}$  denote the number of discretization steps, and let  $0 = t_0 < t_1 < \dots < t_N = 1$  be the sampling grid. We write the uncontrolled reverse update from  $t_i$  to  $t_{i-1}$  as

$$X_{i-1} = \Phi_i^\theta(X_i, \varepsilon_i), \quad \varepsilon_i \sim \mathcal{N}(0, I_d), \quad i = 1, \dots, N, \quad (6)$$

where  $\Phi_i^\theta : \mathbb{R}^d \times \mathbb{R}^d \rightarrow \mathbb{R}^d$  denotes the  $i$ -th denoising transition of the chosen sampler. This covers standard sampling schemes such as DDPM [28] as well as deterministic or higher-order solvers.

To control generation, we perturb each uncontrolled transition by an Euler discretization of the control input over  $[t_{i-1}, t_i]$ , yielding the *discrete-time* version of the stochastic optimal control problem

$$\begin{aligned} \min_{\{X_i\}_{i=0}^N, \{u_i\}_{i=1}^N} \quad & \mathbb{E} \left[ \lambda C(X_0) + \frac{1}{2} \sum_{i=1}^N \|u_i(X_i)\|_2^2 \Delta t_i \right] \\ \text{s.t.} \quad & X_0 \in \mathcal{S}, \quad X_{i-1} = \Phi_i^\theta(X_i, \varepsilon_i) + g_i u_i(X_i) \Delta t_i, \quad \varepsilon_i \sim \mathcal{N}(0, I_d), \quad i = 1, \dots, N, \end{aligned} \quad (7)$$

Although discretization yields a finite-horizon control problem, the discrete SOC optimization remains computationally prohibitive for most diffusion-based applications. The decision variables are feedback controls over  $\mathbb{R}^d$ , while the objective requires an expectation over all controlled stochastic trajectories. In addition, terminal constraints and costs couple all optimization variables with multi-step nonconvex neural dynamics, distorting the optimization landscape to the point that, even for a single noise realization, off-the-shelf solvers may struggle to find feasible solutions.

To tackle these limitations, we simplify the SOC formulation by introducing two additional approximations. First, we adopt a model predictive control (MPC) perspective, replacing the full-horizon problem with a sequence of one-step subproblems. To do so, we exploit the structure of diffusion models and use Tweedie’s formula to construct proxy estimates of the terminal cost-to-go and terminal feasibility condition:

$$\mathbb{E}[C(X_0) \mid X_i] \approx C(\hat{x}_0^\theta(X_i, t_i)), \quad \hat{x}_0^\theta(X_i, t_i) \in \mathcal{S}, \quad i = 0, \dots, N-1. \quad (8)$$

Second, to avoid repeatedly solving constrained optimization problems through the neural denoising map, we approximately invert Tweedie’s formula by a fixed-point argument. This allows us to replace the latent displacement  $X_i - \bar{X}_i$  with a scaled difference between predicted clean samples:

$$X_i - \bar{X}_i \approx \alpha_{t_i} (\hat{x}_0^\theta(X_i, t_i) - \hat{x}_0^\theta(\bar{X}_i, t_i)). \quad (9)$$

---

**Algorithm 1:** DiRecT: Safe diffusion-based planning

---

**Input:** Learned score matching model  $s_t^\theta(\cdot)$ , cost  $C(\cdot)$ , cost weight  $\lambda > 0$ , feasible set  $\mathcal{S}$ , discretization steps  $N$ , time grid  $0 = t_0 < t_1 < \dots < t_N = 1$ , sampling scheme  $\{\Phi_i^\theta\}_{i=1}^N$ , differentiable affine scheduler  $(\alpha_t, \sigma_t)$ .

**Output:** Safe plan  $X_0^*$ .

```
1  $X_N^* \sim \mathcal{N}(0, I_d)$ ; // Sample prior
2 for  $i = N, \dots, 1$  do
3    $\Delta t_i \leftarrow t_i - t_{i-1}$ ; // Time step
4    $\varepsilon_i \sim \mathcal{N}(0, I_d)$ ; // Reverse noise
5    $g_i \leftarrow \left( \frac{d}{dt} \sigma_t^2 - 2 \frac{\dot{\alpha}_t}{\alpha_t} \sigma_t^2 \right)^{1/2} \Big|_{t=t_i}$ ; // Diffusion coefficient
6    $\bar{X}_{i-1}^{\varepsilon_i} \leftarrow \Phi_i^\theta(X_i^*, \varepsilon_i)$ ; // Uncontrolled denoising proposal
7    $\tilde{X}_{0|i-1} \leftarrow \hat{x}_0^\theta(\bar{X}_{i-1}^{\varepsilon_i}, t_{i-1})$ ; // Tweedie clean-sample estimate
8   Solve the constrained subproblem;
9    $\hat{X}_{0|i-1}^* \in \arg \min_{\hat{X}_{0|i-1} \in \mathcal{S}} \lambda C(\hat{X}_{0|i-1}) + \frac{\alpha_{t_{i-1}}^2}{2g_i^2 \Delta t_i} \|\hat{X}_{0|i-1} - \tilde{X}_{0|i-1}\|_2^2$ ; (10)
   if  $i > 1$  then
10     $X_{i-1}^* \leftarrow \bar{X}_{i-1}^{\varepsilon_i} + \alpha_{t_{i-1}}(\hat{X}_{0|i-1}^* - \tilde{X}_{0|i-1})$ ; // Latent correction
11  else
12     $X_0^* \leftarrow \hat{X}_{0|0}^*$ ; // Return feasible terminal sample
13 return  $X_0^*$ 
```

---

Together, these approximations move the one-step constrained optimization from the latent space to the data domain, where the cost and constraint are evaluated directly on the predicted clean sample. We provide the full derivation from Problem 1 to the final algorithm in Appendix C, including all assumptions and approximations. We summarize the complete sampling procedure in Algorithm 1.

Although several approximations are introduced to reduce the general stochastic optimal control problem to a tractable form, terminal constraint satisfaction is not relaxed, as formalized in Proposition 1.

**Proposition 1** (Sample feasibility). *Suppose that the final subproblem in Algorithm 1 admits a feasible solution  $\hat{X}_{0|0}^* \in \mathcal{S}$ . Then the final sample returned by the recursion satisfies the terminal constraint.*

*Proof.* By construction, the final step of Algorithm 1 returns  $X_0^* = \hat{X}_{0|0}^*$ . Since the final subproblem imposes  $\hat{X}_{0|0}^* \in \mathcal{S}$ , it follows immediately that the final sample satisfies the constraint  $X_0^* \in \mathcal{S}$ .  $\square$

## 5 Experiments

We seek to evaluate DiRecT to answer the following questions: (i) *Can our method enforce test-time constraints, while retaining task performance?* (ii) *How does DiRecT compare with existing methods in terms of safety, task success, and computational overhead?* (iii) *How flexible is our method in handling equality and inequality constraints, high-dimensional nonconvex constraint sets, and soft rewards or costs?* To answer these questions, we test our method on maze navigation in Maze2D [23], robotic manipulation in D3IL [30], multi-robot motion planning [58], and diverse contact-rich manipulation in PushT [13, 43]. Detailed settings on the experimental setup are provided in Appendix D and additional results and ablations in Appendix E.

### 5.1 Safe maze navigation

First, we test our method on safe maze navigation for the D4RL Maze2D-large environment [23]. In this task, a small ball traverses a planar maze toward a target position, while avoiding additional *test-time* obstacles as depicted in Figure 1. We train a continuous-time diffusion model to sample state-action pairs over the prediction horizon  $H$ , where each state  $s \in \mathbb{R}^4$  includes position and

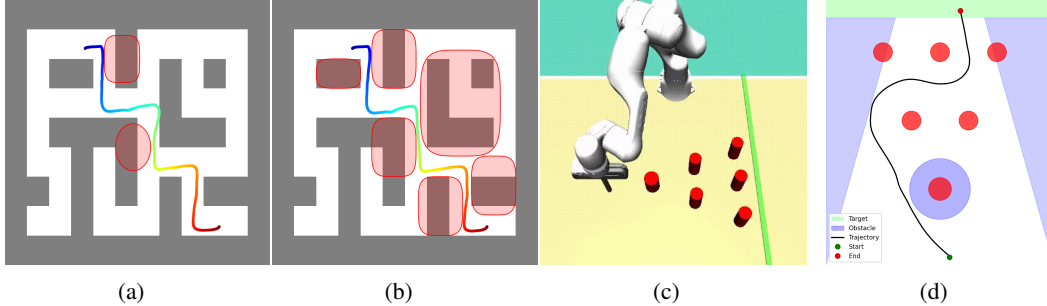


Figure 1: Visualization of DiRecT for maze navigation and robotic manipulation with test-time hard constraints. In Maze2D-broad (1a) and Maze2D-narrow (1b), the robot has to navigate inside a maze toward the bottom-right corner while avoiding the obstacles represented in red. In D3IL-avoiding, a robotic arm moves toward the green target line, while avoiding six pillars (1c). We constrain the problem during inference with additional obstacles, represented in blue (1d).

Table 1: Results on the safe navigation in Maze2D. Mean values over 100 i.i.d. samples and reported alongside their standard deviation. Boldface indicates the best score.

Env	Method	SR $\uparrow$	Violations $\downarrow$	Score $\uparrow$	Time (s) $\downarrow$
Maze2D Broad	Diffuser [29]	0.000	45.92 $\pm$ 11.86	<b>1.601<math>\pm</math>0.025</b>	0.316 $\pm$ 0.078
	Gradient Guidance [15]	0.040	25.52 $\pm$ 10.18	1.587 $\pm$ 0.164	3.637 $\pm$ 0.076
	Projected Diffusion [14]	0.220	42.00 $\pm$ 47.28	1.119 $\pm$ 0.708	46.398 $\pm$ 11.096
	Augmented Lagrangian [71]	0.080	72.92 $\pm$ 92.75	-0.010 $\pm$ 0.145	5.676 $\pm$ 0.566
	SafeDiffuser-RoS [69]	0.040	66.26 $\pm$ 41.72	1.186 $\pm$ 0.533	148.967 $\pm$ 3.831
	<b>DiRecT (Ours)</b>	<b>0.970</b>	<b>0.45<math>\pm</math>3.81</b>	1.500 $\pm$ 0.419	17.657 $\pm$ 0.629
Maze2D Narrow	Diffuser [29]	0.000	103.94 $\pm$ 21.88	1.601 $\pm$ 0.025	0.321 $\pm$ 0.086
	Gradient Guidance [15]	0.000	51.30 $\pm$ 19.22	1.619 $\pm$ 0.0029	3.608 $\pm$ 0.023
	Projected Diffusion [14]	0.780	37.29 $\pm$ 129.88	0.163 $\pm$ 0.459	112.918 $\pm$ 19.517
	Augmented Lagrangian [71]	0.000	217.51 $\pm$ 159.43	0.156 $\pm$ 0.449	6.022 $\pm$ 0.122
	SafeDiffuser-RoS [69]	0.000	278.87 $\pm$ 209.87	0.735 $\pm$ 0.681	509.850 $\pm$ 19.929
	<b>DiRecT (Ours)</b>	<b>0.940</b>	<b>0.23<math>\pm</math>1.04</b>	<b>1.624<math>\pm</math>0.027</b>	98.093 $\pm$ 5.047

velocity of the ball and actions  $a \in \mathbb{R}^2$  represent force inputs. During inference, we sample *one* trajectory from the model conditioned on endpoint states and execute actions by tracking with a proportional-derivative (PD) controller. Although the sampled *planned* trajectory may satisfy test-time constraints, the *rollout* trajectory can deviate from the plan and become infeasible due to mismatch between learned and environment dynamics. To improve rollout fidelity [9, 55], we impose additional *equality* constraints in the form of linearized dynamics fitted from the training data (see Appendix D.1).

**Baselines.** We compare against five baselines to represent different classes of constrained planners: **Diffuser** [29] (unguided reference), **Gradient Guidance** [15] (soft constraining with posterior sampling), **Projected Diffusion** [14] (per-step projection), **Augmented Lagrangian** [71] (early-stage Lagrangian constraint relaxation), and **SafeDiffuser-RoS** [69] (CBF-based guidance). We adapt existing methods to include dynamic constraints and employ IPOPT [68] as an *off-the-shelf* solver. Additional results are provided in Appendix E.1.

**Evaluation.** We test all methods over two progressively challenging variants [13, 29, 71], which we denote as *broad* (Fig. 1a) and *narrow* (Fig. 1b). For each variant, we evaluate 100 independent trials to measure how well each method adapts to additional prior environment knowledge in the form of dynamic constraints for safe navigation. We report in Table 1 four evaluation metrics: *Safety Rate* (SR), the fraction of collision-free rollouts; *Violations*, the mean number of steps the ball spends inside obstacles; D4RL normalized *Score*, which reflects task completion performance; and sampling *Time*. DiRecT is the only method that achieves high safety and near-zero violations while retaining strong performance.

Table 2: Results on constrained manipulation in D3IL *avoiding*. Mean values are computed over 100 i.i.d. trials and reported with standard deviations where applicable. Boldface indicates the best score.

Env	Method	SR $\uparrow$	Task Success $\uparrow$	Steps (Safe) $\downarrow$	Time (s) $\downarrow$
D3IL Avoiding	Unconstrained Diffuser [29]	0.060	0.960	70.30 $\pm$ 11.83	0.224 $\pm$ 0.002
	Gradient Guidance [15]	0.880	0.980	<b>62.58<math>\pm</math>7.05</b>	6.615 $\pm$ 0.540
	Projected Diffusion [14]	0.770	0.970	63.77 $\pm$ 6.88	1.367 $\pm$ 0.057
	Augmented Lagrangian [71]	0.220	0.840	63.45 $\pm$ 7.22	4.152 $\pm$ 0.018
	SafeDiffuser-RoS [69]	0.370	0.820	63.19 $\pm$ 11.56	18.890 $\pm$ 0.877
	<b>DiRecT (Ours)</b>	<b>1.000</b>	<b>1.000</b>	62.86 $\pm$ 6.90	0.688 $\pm$ 0.061

## 5.2 Safe robotic manipulation

We next evaluate the reliability and performance of our method for closed-loop robotic manipulation on the D3IL *avoiding* environment [30]. In this task, a robotic manipulator moves toward a target region while its end-effector avoids six pillars (Fig. 1c). We train a continuous-time diffusion model on the D3IL demonstration dataset, consisting of expert state-action trajectories, where the robot state  $s \in \mathbb{R}^4$  is composed of the current and desired positions, and the action  $a \in \mathbb{R}^2$  represents the end-effector velocity. At test time, the end-effector must reach the target region while avoiding the environment pillars and *additional* planar and circular constraints (Fig. 1d). Rollouts are performed in a receding-horizon fashion, in which we execute  $M < H$  actions before re-planning. Similarly to the maze navigation task, we test the ability of our method to exploit additional environment priors in the form of linearized dynamic constraints.

**Baselines.** We compare against the same baselines as in the Maze2D setting. Additional results and baselines are presented in Appendix E.2.

**Evaluation.** We test each method over 100 i.i.d. rollouts and compute the following metrics: *Safety Rate* (SR), the fraction of trials satisfying both environment and test-time constraints; *Task Success* (TS), the proportion of trajectories that reach the end goal in the allowed number of steps; average *Steps* taken to reach the target for safe rollouts; sampling *Time*. Results in Table 2 show that our method is the only one to maintain performance and safety for *all* initializations.

## 5.3 Safe multi-robot motion planning

We test DiRecT on the coupled diffusion generation benchmark of [43], which is based on the multi-robot motion planning (MRMP) environment introduced by [58]. Given starting locations for each robot, the goal is to simultaneously sample trajectories for all robots from a diffusion model trained on single-agent examples, while avoiding *inter-robot* and *obstacle* collisions, satisfying inference-time *velocity* constraints, and exhibiting target environment-specific behaviors (Figure 2). Given the high-dimensional and nonconvex nature of the MRMP problem, we test the robustness of different methods by scaling the number of agents up to twenty, while imposing velocity limits as in [43].

**Baselines.** We compare our method with the following references: **Diffuser** [29] (unconstrained reference), **MMD-CBS** [58] (tree-search collision search without velocity constraints), **PCD-LB** and **PCD-SHD** [43] (soft guidance for collision avoidance and projection for velocity feasibility). For fast and parallelizable projection of trajectories onto the nonconvex feasible set, we develop a custom *domain-specific* optimizer that is amenable to just-in-time compilation and GPU parallelization in JAX [11] (see Appendix D.3.1). To show that the interplay between the generative process and projection optimization is integral to the success and reliability of the algorithm, we implement **Final Projection**, in which samples are generated unconditionally and then projected *post-sampling* onto the feasible set.

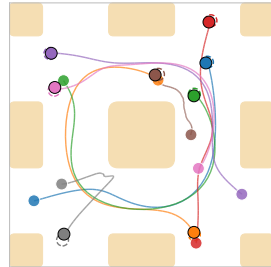


Figure 2: Highways with 8 agents. Desired motion is counterclockwise around the central obstacle.

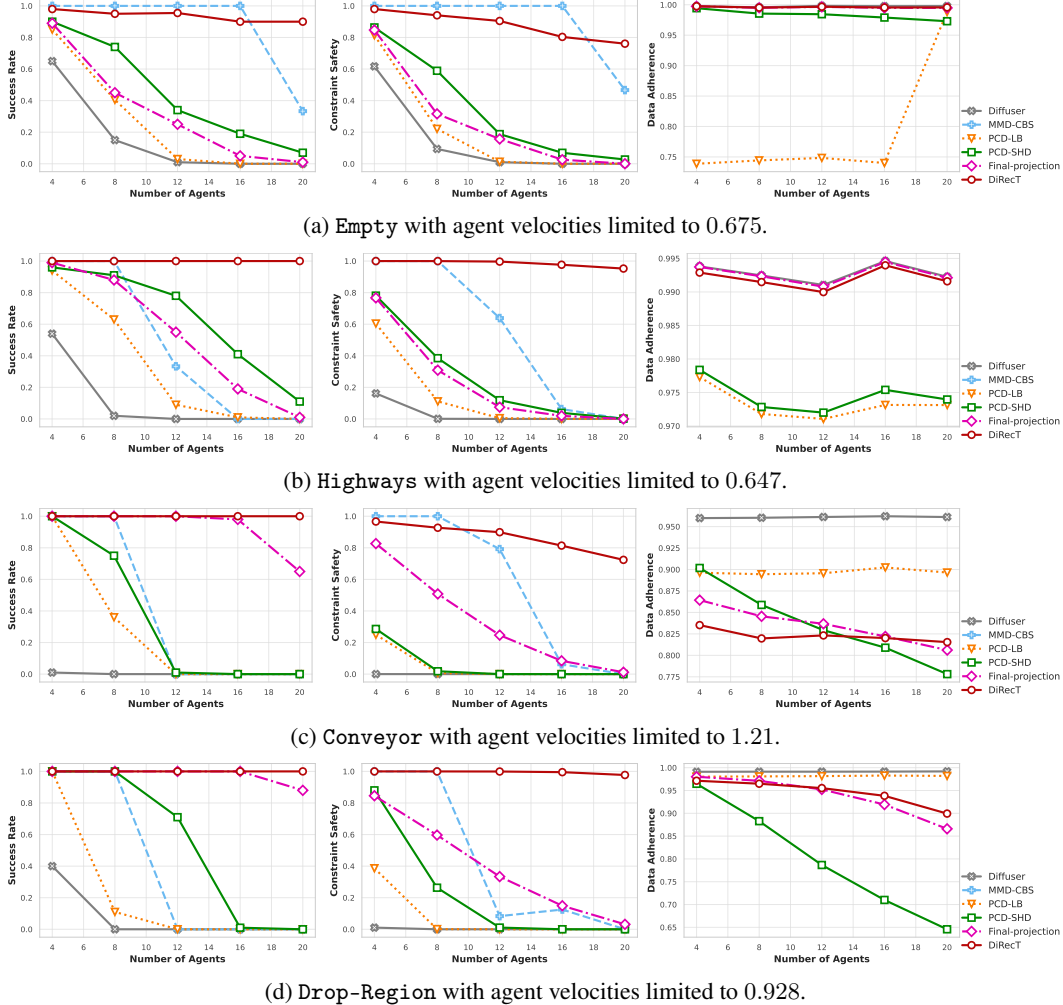


Figure 3: Performance comparison for  $N \in \{4, 8, 12, 16, 20\}$  agents on the four MMD environments [58]. We impose obstacle and inter-robot constraints and restrict agent velocities. Our method outperforms all other baselines in terms of safety, while maintaining adherence to the expected motion pattern.

**Evaluation.** We assess each method over 100 starting configurations, generating 128 candidate trajectories for each initialization as in [43]. We report the following metrics: *Success Rate*, which is the fraction of trials with at least one collision-free trajectory among the generated candidate trajectories; *Constraint Safety*, which is the proportion of *all* samples satisfying collision and kinematic constraints, and *Data Adherence*, which measures environment-specific task success. As shown in Figure 3, DiRecT outperforms all other baselines in terms of safety, especially when scaling to twenty agents. Note that the relatively lower data adherence on Conveyor is not representative of a relative lack of performance, as all other baselines mostly generate infeasible samples. We provide additional experimentation details in Appendix D.3 and extensive sweep results in Appendix E.3.

## 5.4 Safe and diverse contact-rich manipulation

Finally, we show that DiRecT can effectively incorporate and optimize over *soft* costs while satisfying test-time constraints. We base our evaluation on simultaneous coupled trajectory generation on PushT [22]. In the single-agent setting, the objective is to push a T-shaped block from a randomized starting position until it overlaps with a target pose (Figure 4). Following [43], we consider the simultaneous generation of a pair of distinct trajectories while imposing *hard* constraints on the maximum velocity and *soft* coupling costs to encourage non-intersecting, diverse trajectories.

Table 3: Results on generation of safe and diverse contact-rich manipulation in PushT, with a velocity limit of 8.4. Best overall value(s) in boldface; underlining denotes best among constrained samplers.

Method	DTW $\uparrow$	DFD $\uparrow$	CS $\uparrow$	TC $\uparrow$	Time (s) $\downarrow$
Diffusion Policy [13]	3.26 $\pm$ 1.280	0.477 $\pm$ 0.167	0.6549 $\pm$ 0.098	<b>0.928<math>\pm</math>0.194</b>	0.136 $\pm$ 0.015
CD-LB [43]	<b>4.242<math>\pm</math>1.292</b>	<b>0.610<math>\pm</math>0.166</b>	0.592 $\pm$ 0.136	0.907 $\pm$ 0.209	0.138 $\pm$ 0.006
CD-DPP [43]	3.871 $\pm$ 1.169	0.560 $\pm$ 0.150	0.632 $\pm$ 0.134	0.921 $\pm$ 0.207	0.142 $\pm$ 0.010
PCD-LB [43]	3.928 $\pm$ 1.238	0.557 $\pm$ 0.159	<u>1.000<math>\pm</math>0.000</u>	0.890 $\pm$ 0.226	0.490 $\pm$ 0.008
PCD-DPP [43]	3.530 $\pm$ 1.236	0.503 $\pm$ 0.160	<u>1.000<math>\pm</math>0.000</u>	0.898 $\pm$ 0.224	0.492 $\pm$ 0.008
DiRecT-LB	4.046 $\pm$ 1.139	0.581 $\pm$ 0.146	<u>1.000<math>\pm</math>0.000</u>	<u>0.924<math>\pm</math>0.190</u>	0.373 $\pm$ 0.008
DiRecT-DPP	<u>4.226<math>\pm</math>1.126</u>	<u>0.609<math>\pm</math>0.142</u>	<u>1.000<math>\pm</math>0.000</u>	0.913 $\pm$ 0.207	0.372 $\pm$ 0.008

**Baselines.** We compare against vanilla **Diffusion Policy** [13], Projected Coupled Diffusion variants with Determinantal Point Process (DPP) and Log-barrier (LB) losses, both without velocity projection (**CD-DPP**, **CD-LB** [43]) and with velocity projection (**PCD-DPP**, **PCD-LB** [43]). To demonstrate that our method can improve diversity with the same computational overhead, we incorporate DPP and LB costs into (10), and solve the resulting optimization with one step of Projected Gradient Descent [37], thereby requiring one projection and one gradient computation per sampling step (see Appendix D.4). We denote the two variants of our method as **DiRecT-DPP** and **DiRecT-LB**.

**Evaluation.** We follow the same experimental procedure, generating 100 *pairs* of trajectories over 50 random initializations for the block and agent positions and report the following metrics: *Dynamic Time Warping* (DTW) [6, 46] and *Discrete Fréchet Distance* (DFD) [2] to evaluate diversity; *Task Completion* score (TC) [13, 22], measuring successful overlap of the blocks onto the respective targets; *Constraint Satisfaction* rate (CS) [43] as the fraction of samples satisfying velocity limits; and sampling *Time*. As summarized in Table 3, our formulation improves both diversity and task success relative to other constrained baselines, highlighting the importance of performing both *soft* and *hard* guidance near the data manifold. As observed by [43], diversity objectives conflict with task completion, leading to Pareto-optimal solutions as a function of guidance strength. In Appendix E.4, we show that DiRecT dominates PCD in terms of Pareto optimality.

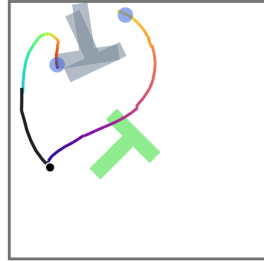


Figure 4: Coupled generation on PushT. Two agents push gray blocks onto a green target pose while avoiding intersecting trajectories.

## 6 Conclusion

In this paper, we introduced DiRecT, a training-free algorithm for constrained sampling in safe diffusion-based planning. By formulating constrained sampling as a terminally constrained stochastic optimal control problem and deriving a scalable receding-horizon surrogate, DiRecT separates stochastic denoising from trajectory-level constraint satisfaction. This design avoids overconstraining noisy intermediate iterates while retaining the flexibility to incorporate domain-specific optimizers, dynamics priors, and additional soft objectives. Experiments across diverse robotic planning domains demonstrate that DiRecT improves both constraint satisfaction and task success, highlighting its potential for reliable deployment in safety-critical planning tasks.

**Limitations and future work.** Our method enforces hard constraints for pretrained diffusion planners in a *training-free* manner, making it broadly applicable to existing models without retraining. This flexibility, however, comes with additional inference-time computation. A natural direction for future work is to combine terminal constraint control with model fine-tuning, reducing runtime overhead and improving adaptability to test-time constraints.

## References

- [1] Anurag Ajay, Yilun Du, Abhi Gupta, Joshua Tenenbaum, Tommi Jaakkola, and Pulkit Agrawal. Is conditional generative modeling all you need for decision-making? In *International Conference on Learning Representations*, 2023.
- [2] Helmut Alt and Michael Godau. Computing the fréchet distance between two polygonal curves. *International Journal of Computational Geometry & Applications*, 5(01n02):75–91, 1995.
- [3] Brian D.O. Anderson. Reverse-time diffusion equation models. *Stochastic Processes and their Applications*, 12(3):313–326, 1982. ISSN 0304-4149. doi: [https://doi.org/10.1016/0304-4149\(82\)90051-5](https://doi.org/10.1016/0304-4149(82)90051-5). URL <https://www.sciencedirect.com/science/article/pii/0304414982900515>.
- [4] Joel A E Andersson, Joris Gillis, Greg Horn, James B Rawlings, and Moritz Diehl. CasADi – A software framework for nonlinear optimization and optimal control. *Mathematical Programming Computation*, 11(1):1–36, 2019. doi: 10.1007/s12532-018-0139-4.
- [5] Richard Bellman. The theory of dynamic programming. Paper P-550, RAND Corporation, Santa Monica, CA, 1954. URL <https://www.rand.org/pubs/papers/P550.html>.
- [6] Donald J Berndt and James Clifford. Using dynamic time warping to find patterns in time series. In *Proceedings of the 3rd international conference on knowledge discovery and data mining*, pages 359–370, 1994.
- [7] Dimitri P. Bertsekas and John N. Tsitsiklis. *Neuro-Dynamic Programming*. Athena Scientific, 1996.
- [8] Bruno Bouchard, Romuald Elie, and Cyril Imbert. Optimal control under stochastic target constraints. *SIAM Journal on Control and Optimization*, 48(5):3501–3531, 2010.
- [9] Jean-Baptiste Bouvier, Kanghyun Ryu, Kartik Nagpal, Qiayuan Liao, Koushil Sreenath, and Negar Mehr. Ddat: Diffusion policies enforcing dynamically admissible robot trajectories. In *Robotics: Science and Systems (RSS)*, 2025.
- [10] Stephen Boyd, Neal Parikh, Eric Chu, Borja Peleato, and Jonathan Eckstein. Distributed optimization and statistical learning via the alternating direction method of multipliers. *Foundations and Trends in Machine Learning*, 3(1):1–122, 2011.
- [11] James Bradbury, Roy Frostig, Peter Hawkins, Matthew James Johnson, Yash Katriya, Chris Leary, Dougal Maclaurin, George Necula, Adam Paszke, Jake VanderPlas, Skye Wanderman-Milne, and Qiao Zhang. JAX: composable transformations of Python+NumPy programs, 2018. URL <http://github.com/jax-ml/jax>.
- [12] Luiz F Chamon, Mohammad R Karimi, and Anna Korba. Constrained sampling with primal-dual langevin monte carlo. *Advances in Neural Information Processing Systems*, 37:29285–29323, 2024.
- [13] Cheng Chi, Zhenjia Xu, Siyuan Feng, Eric Cousineau, Yilun Du, Benjamin Burchfiel, Russ Tedrake, and Shuran Song. Diffusion policy: Visuomotor policy learning via action diffusion. *The International Journal of Robotics Research*, 44(10-11):1684–1704, 2025.
- [14] Jacob K Christopher, Stephen Baek, and Ferdinando Fioretto. Constrained synthesis with projected diffusion models. *Advances in Neural Information Processing Systems*, 37:89307–89333, 2024.
- [15] Hyungjin Chung, Jeongsol Kim, Michael T. Mccann, Marc L. Klasky, and Jong Chul Ye. Diffusion posterior sampling for general noisy inverse problems. In *International Conference on Learning Representations*, 2023.
- [16] Xiaobing Dai, Zewen Yang, Dian Yu, Fangzhou Liu, Hamid Sadeghian, Sami Haddadin, and Sandra Hirche. Safeflow: Safe robot motion planning with flow matching via control barrier functions, 2025. URL <https://arxiv.org/abs/2504.08661>.

- [17] Prafulla Dhariwal and Alexander Nichol. Diffusion models beat gans on image synthesis. In *Advances in Neural Information Processing Systems*, volume 34, pages 8780–8794, 2021.
- [18] Carles Domingo-Enrich, Michal Drozdal, Brian Karrer, and Ricky TQ Chen. Adjoint matching: Fine-tuning flow and diffusion generative models with memoryless stochastic optimal control. *arXiv preprint arXiv:2409.08861*, 2024.
- [19] Chenyou Fan, Chenjia Bai, Zhao Shan, Haoran He, Yang Zhang, and Zhen Wang. Task-agnostic pre-training and task-guided fine-tuning for versatile diffusion planner. *arXiv preprint arXiv:2409.19949*, 2024.
- [20] Zeyu Feng, Hao Luan, Pranav Goyal, and Harold Soh. Ltldog: Satisfying temporally-extended symbolic constraints for safe diffusion-based planning. *IEEE Robotics and Automation Letters*, 9(10):8571–8578, 2024. doi: 10.1109/LRA.2024.3443501.
- [21] Wendell H Fleming and Raymond W Rishel. *Deterministic and stochastic optimal control*. Springer Science & Business Media, 2012.
- [22] Pete Florence, Corey Lynch, Andy Zeng, Oscar A Ramirez, Ayzaan Wahid, Laura Downs, Adrian Wong, Johnny Lee, Igor Mordatch, and Jonathan Tompson. Implicit behavioral cloning. In *5th Annual Conference on Robot Learning*, 2021. URL <https://openreview.net/forum?id=rif3a5NAXU6>.
- [23] Justin Fu, Aviral Kumar, Ofir Nachum, George Tucker, and Sergey Levine. D4rl: Datasets for deep data-driven reinforcement learning, 2020.
- [24] Jiequn Han, Arnulf Jentzen, and Weinan E. Solving high-dimensional partial differential equations using deep learning. *Proceedings of the National Academy of Sciences*, 115(34): 8505–8510, 2018.
- [25] Peter E. Hart, Nils J. Nilsson, and Bertram Raphael. A formal basis for the heuristic determination of minimum cost paths. *IEEE Transactions on Systems Science and Cybernetics*, 4(2): 100–107, 1968. doi: 10.1109/TSSC.1968.300136.
- [26] U. G. Haussmann and J. P. Lepeltier. On the existence of optimal controls. *SIAM Journal on Control and Optimization*, 28(4):851–902, 1990. doi: 10.1137/0328049.
- [27] Jonathan Ho and Tim Salimans. Classifier-free diffusion guidance. In *NeurIPS 2021 Workshop on Deep Generative Models and Downstream Applications*, 2021. URL <https://openreview.net/forum?id=qw8AKxfYbI>.
- [28] Jonathan Ho, Ajay Jain, and Pieter Abbeel. Denoising diffusion probabilistic models. In *Advances in Neural Information Processing Systems*, volume 33, pages 6840–6851, 2020.
- [29] Michael Janner, Yilun Du, Joshua B. Tenenbaum, and Sergey Levine. Planning with diffusion for flexible behavior synthesis. In *Proceedings of the 39th International Conference on Machine Learning*, volume 162 of *Proceedings of Machine Learning Research*, pages 9902–9915, 2022.
- [30] Xiaogang Jia, Denis Blessing, Xinkai Jiang, Moritz Reuss, Atalay Donat, Rudolf Lioutikov, and Gerhard Neumann. Towards diverse behaviors: A benchmark for imitation learning with human demonstrations. In *The Twelfth International Conference on Learning Representations*, 2024. URL <https://openreview.net/forum?id=6pPYRXKPPw>.
- [31] Hilbert J. Kappen. Path integrals and symmetry breaking for optimal control theory. *Journal of Statistical Mechanics: Theory and Experiment*, 2005(11):P11011, 2005.
- [32] Sertac Karaman and Emilio Frazzoli. Sampling-based algorithms for optimal motion planning. *The International Journal of Robotics Research*, 30(7):846–894, 2011. doi: 10.1177/0278364911406761.
- [33] L.E. Kavraki, P. Svestka, J.-C. Latombe, and M.H. Overmars. Probabilistic roadmaps for path planning in high-dimensional configuration spaces. *IEEE Transactions on Robotics and Automation*, 12(4):566–580, 1996. doi: 10.1109/70.508439.

- [34] Diederik P Kingma and Jimmy Ba. Adam: A method for stochastic optimization. *arXiv preprint arXiv:1412.6980*, 2014.
- [35] Peter E. Kloeden and Eckhard Platen. *Numerical Solution of Stochastic Differential Equations*. Springer, 1992.
- [36] Steven LaValle. Rapidly-exploring random trees: A new tool for path planning. *Research Report 9811*, 1998.
- [37] Evgeny S. Levitin and Boris T. Polyak. Constrained minimization methods. *USSR Computational Mathematics and Mathematical Physics*, 6(5):1–50, 1966.
- [38] Zeyang Li, Kaveh Alim, and Navid Azizan. Hardflow: Hard-constrained sampling for flow-matching models via trajectory optimization. *arXiv preprint arXiv:2511.08425*, 2025.
- [39] Jinhao Liang, Jacob K Christopher, Sven Koenig, and Ferdinando Fioretto. Simultaneous multi-robot motion planning with projected diffusion models. In *Forty-second International Conference on Machine Learning*, 2025. URL <https://openreview.net/forum?id=Sp7jc1UwkV>.
- [40] Zhixuan Liang, Yao Mu, Mingyu Ding, Fei Ni, Masayoshi Tomizuka, and Ping Luo. Adaptdiffuser: Diffusion models as adaptive self-evolving planners. *arXiv preprint arXiv:2302.01877*, 2023.
- [41] Cheng Lu, Yuhao Zhou, Fan Bao, Jianfei Chen, Chongxuan Li, and Jun Zhu. DPM-Solver: A fast ode solver for diffusion probabilistic model sampling in around 10 steps. In *Advances in Neural Information Processing Systems*, 2022.
- [42] Cheng Lu, Yuhao Zhou, Fan Bao, Jianfei Chen, Chongxuan Li, and Jun Zhu. Dpm-solver++: Fast solver for guided sampling of diffusion probabilistic models. *Machine Intelligence Research*, 22(4):730–751, 2025.
- [43] Hao Luan, Yi Xian Goh, See-Kiong Ng, and Chun Kai Ling. Projected coupled diffusion for test-time constrained joint generation. In *The Fourteenth International Conference on Learning Representations*, 2026. URL <https://openreview.net/forum?id=1FE5JLpvg>.
- [44] Yuanqi Mao, Michael Szmuk, Xiangru Xu, and Behçet Açıkmeşe. Successive convexification: A superlinearly convergent algorithm for non-convex optimal control problems. *arXiv preprint arXiv:1804.06539*, 2018.
- [45] Kazuki Mizuta and Karen Leung. Cobl-diffusion: Diffusion-based conditional robot planning in dynamic environments using control barrier and lyapunov functions. In *2024 IEEE/RSJ International Conference on Intelligent Robots and Systems (IROS)*, pages 13801–13808. IEEE, 2024.
- [46] Meinard Müller. *Information retrieval for music and motion*. Springer, 2007.
- [47] Alexander Quinn Nichol and Prafulla Dhariwal. Improved denoising diffusion probabilistic models. In *Proceedings of the 38th International Conference on Machine Learning*, pages 8162–8171. PMLR, 2021.
- [48] Kushagra Pandey, Farrin Marouf Sofian, Felix Draxler, Theofanis Karaletsos, and Stephan Mandt. Variational control for guidance in diffusion models. In *Forty-second International Conference on Machine Learning*, 2025. URL <https://openreview.net/forum?id=Z0ffRRt0im>.
- [49] Adam Paszke, Sam Gross, Soumith Chintala, Gregory Chanan, Edward Yang, Zachary DeVito, Zeming Lin, Alban Desmaison, Luca Antiga, and Adam Lerer. Automatic differentiation in pytorch. In *NIPS-W*, 2017.
- [50] Thomas Power, Rana Soltani-Zarrin, Soshi Iba, and Dmitry Berenson. Sampling constrained trajectories using composable diffusion models. In *IROS 2023 Workshop on Differentiable Probabilistic Robotics: Emerging Perspectives on Robot Learning*, 2023. URL <https://openreview.net/forum?id=UAylEpIMNE>.

- [51] Nathan Ratliff, Matt Zucker, J. Andrew Bagnell, and Siddhartha Srinivasa. Chomp: Gradient optimization techniques for efficient motion planning. In *2009 IEEE International Conference on Robotics and Automation*, pages 489–494, 2009. doi: 10.1109/ROBOT.2009.5152817.
- [52] James B. Rawlings, David Q. Mayne, and Moritz M. Diehl. *Model Predictive Control: Theory, Computation, and Design*. Nob Hill Publishing, 2017.
- [53] Allen Z Ren, Justin Lidard, Lars L Ankile, Anthony Simeonov, Pulkit Agrawal, Anirudha Majumdar, Benjamin Burchfiel, Hongkai Dai, and Max Simchowitz. Diffusion policy optimization. *arXiv preprint arXiv:2409.00588*, 2024.
- [54] Herbert Robbins. An empirical bayes approach to statistics. *Breakthroughs in Statistics*, pages 388–394, 1992.
- [55] Ralf Römer, Alexander von Rohr, and Angela Schoellig. Diffusion predictive control with constraints. In *Proceedings of the 7th Annual Learning for Dynamics & Control Conference*, pages 791–803. PMLR, 2025.
- [56] Litu Rout, Yujia Chen, Nataniel Ruiz, Abhishek Kumar, Constantine Caramanis, Sanjay Shakkottai, and Wen-Sheng Chu. RB-modulation: Training-free stylization using reference-based modulation. In *The Thirteenth International Conference on Learning Representations*, 2025. URL <https://openreview.net/forum?id=bnINPG5A32>.
- [57] John Schulman, Yan Duan, Jonathan Ho, Alex Lee, Ibrahim Awwal, Henry Bradlow, Jia Pan, Sachin Patil, Ken Goldberg, and Pieter Abbeel. Motion planning with sequential convex optimization and convex collision checking. *The International Journal of Robotics Research*, 33(9):1251–1270, 2014.
- [58] Yorai Shaoul, Itamar Mishani, Shivam Vats, Jiaoyang Li, and Maxim Likhachev. Multi-robot motion planning with diffusion models. In *The Thirteenth International Conference on Learning Representations*, 2025. URL <https://openreview.net/forum?id=AUCYptvAf3>.
- [59] Justin Sirignano and Konstantinos Spiliopoulos. DGM: A deep learning algorithm for solving partial differential equations. *Journal of Computational Physics*, 375:1339–1364, 2018.
- [60] Jascha Sohl-Dickstein, Eric A. Weiss, Niru Maheswaranathan, and Surya Ganguli. Deep unsupervised learning using nonequilibrium thermodynamics. In *Proceedings of the 32nd International Conference on Machine Learning*, volume 37 of *Proceedings of Machine Learning Research*, pages 2256–2265, 2015.
- [61] Jiaming Song, Chenlin Meng, and Stefano Ermon. Denoising diffusion implicit models. In *International Conference on Learning Representations*, 2021. URL <https://openreview.net/forum?id=StgiarCHLP>.
- [62] Yang Song, Jascha Sohl-Dickstein, Diederik P. Kingma, Abhishek Kumar, Stefano Ermon, and Ben Poole. Score-based generative modeling through stochastic differential equations. In *International Conference on Learning Representations*, 2021.
- [63] Richard S. Sutton and Andrew G. Barto. *Reinforcement Learning: An Introduction*. MIT Press, 2 edition, 2018.
- [64] Evangelos A. Theodorou and Emanuel Todorov. Relative entropy and free energy dualities: Connections to path integral and KL control. In *Proceedings of the IEEE Conference on Decision and Control (CDC)*, pages 1466–1473. IEEE, 2012.
- [65] Francisco Vargas, Will Sussman Grathwohl, and Arnaud Doucet. Denoising diffusion samplers. In *The Eleventh International Conference on Learning Representations*, 2023. URL <https://openreview.net/forum?id=8pvnfTAbu1f>.
- [66] Francisco Vargas, Shreyas Padhy, Denis Blessing, and Nikolas Nüsken. Transport meets variational inference: Controlled monte carlo diffusions. In *The Twelfth International Conference on Learning Representations*, 2024. URL <https://openreview.net/forum?id=PP1rudnxiW>.

- [67] Pascal Vincent. A connection between score matching and denoising autoencoders. *Neural Computation*, 23(7):1661–1674, 2011.
- [68] Andreas Wächter and Lorenz T. Biegler. On the implementation of an interior-point filter line-search algorithm for large-scale nonlinear programming. *Mathematical Programming*, 106(1):25–57, 2006. doi: 10.1007/s10107-004-0559-y.
- [69] Wei Xiao, Tsun-Hsuan Wang, Chuang Gan, Ramin Hasani, Mathias Lechner, and Daniela Rus. Safediffuser: Safe planning with diffusion probabilistic models. In *The Thirteenth International Conference on Learning Representations*, 2025. URL <https://openreview.net/forum?id=ig2wk7kK9J>.
- [70] Jingjin Yu. Intractability of optimal multi-robot path planning on planar graphs. *IEEE Robotics and Automation Letters*, 1(1):33–40, 2016. doi: 10.1109/LRA.2015.2503143.
- [71] Jichen Zhang, Liqun Zhao, Antonis Papachristodoulou, and Jack Umenberger. Constrained diffusers for safe planning and control, 2025. URL <https://arxiv.org/abs/2506.12544>.

# Appendix

<b>A</b>	<b>Related Work</b>	<b>16</b>
<b>B</b>	<b>Stochastic optimal control and constrained sampling</b>	<b>17</b>
<b>C</b>	<b>Algorithm derivation</b>	<b>19</b>
<b>D</b>	<b>Implementation details</b>	<b>21</b>
	D.1 Safe maze navigation . . . . .	22
	D.2 Safe robotic manipulation . . . . .	23
	D.3 Safe multi-robot motion planning . . . . .	23
	D.4 Safe and diverse contact-rich manipulation . . . . .	28
<b>E</b>	<b>Additional results</b>	<b>29</b>
	E.1 Safe maze navigation . . . . .	29
	E.2 Safe robotic manipulation . . . . .	30
	E.3 Safe multi-robot motion planning . . . . .	31
	E.4 Safe and diverse contact-rich manipulation . . . . .	33
<b>F</b>	<b>Visualizations</b>	<b>34</b>

---

## A Related Work

**Safe diffusion-based planning.** Existing approaches to diffusion-based planning with test-time constraint enforcement can largely be understood through the lens of projection, differing primarily in *when* projection is applied and how strongly it restricts the denoising process. A simple strategy is *post-sampling* projection, where an unconstrained diffusion model first generates a trajectory and feasibility is enforced only afterward. This direction was explored by Power et al. [50]. While conceptually straightforward, post-sampling projection can move samples substantially away from the pretrained diffusion distribution, as observed by Christopher et al. [14]. Most subsequent methods instead perform projection *during* sampling. For example, Christopher et al. [14] formulate constrained sampling as a maximum-likelihood problem in which all intermediate latents are required to lie in the feasible set, and sample using projected stochastic Langevin dynamics. Building on this per-step projection perspective, Luan et al. [43] extend projected diffusion models to multi-robot motion planning with coupled trajectory generation and additional soft costs, while Liang et al. [39] introduce a customized Lagrangian-based projector that relaxes nonconvex collision constraints. Recognizing that enforcing constraints throughout the entire denoising process can be overly restrictive, more recent methods relax early-stage sampling and tighten constraint enforcement near the end of generation. Zhang et al. [71] propose a Lagrangian formulation for safe planning, where constraint strictness is progressively increased through primal-dual or augmented-Lagrangian updates. In a related direction, SafeDiffuser [69] views denoising as a controlled dynamical system and incorporates control barrier functions (CBFs) into the sampling process. This allows constraint violations during early denoising while enforcing terminal feasibility through the CBF condition. However, balancing early-stage relaxation with reliable terminal feasibility can require careful parameter tuning; moreover, even relaxed variants still impose restrictions along the denoising trajectory. Overall, most existing methods share a common feature: constraint satisfaction is enforced through projections or constraint-driven updates along the denoising path. In contrast, our method adopts a stochastic optimal control perspective that imposes hard constraints only on the terminal clean sample, rather than requiring feasibility of noisy intermediate iterates. It instead steers the sampling process toward feasibility of the final trajectory, reducing unnecessary restrictions on the learned diffusion dynamics. Moreover, beyond hard constraints, practical planning problems often involve soft costs or rewards. While projection-based approaches can incorporate such objectives in specific implementations, they do not naturally provide a unified framework for jointly handling hard feasibility and soft optimality. Our stochastic optimal control formulation addresses both within a single inference-time procedure, enabling efficient and flexible constrained sampling.

**Diffusion models and stochastic optimal control.** A growing body of work has connected diffusion sampling with stochastic optimal control (SOC), viewing the reverse diffusion process as a controlled stochastic dynamics whose drift can be modified while penalizing deviations from a reference process. One line of work uses this perspective for sampling from unnormalized target densities, where a reference diffusion process is controlled to match a desired distribution; representative examples include path-integral sampling [31], denoising diffusion samplers [65], and controlled Monte Carlo diffusions [66]. Another line of work applies SOC to reward optimization in generative models, either through training-based reward fine-tuning, such as Adjoint Matching [18], or through training-free guidance toward soft objectives, such as RB-Modulation [56] and variational diffusion guidance [48]. These methods demonstrate the usefulness of the SOC viewpoint for controlling diffusion samplers, but they primarily target distributional sampling or soft reward optimization. They do not directly address hard-constrained planning, where the final trajectory must satisfy feasibility constraints while remaining faithful to the learned diffusion dynamics. Extending SOC-based diffusion control to this setting is nontrivial, and existing reward-guidance methods do not yield an efficient constrained sampler. In contrast, our work develops a tractable surrogate tailored to terminally constrained sampling for diffusion-based planning, enabling efficient inference-time enforcement of hard constraints while also accommodating additional soft costs or rewards.

**Training-based diffusion planners.** A parallel and complementary line of work adapts diffusion-based planners through additional training or fine-tuning. For example, AdaptDiffuser [40] improves diffusion planners via self-evolution, using reward-guided synthetic trajectories to update the model. SODP [19] pretrains a task-agnostic diffusion planner on diverse suboptimal data and then fine-tunes it with task-specific rewards. DPPO [53] further adapts diffusion policies for continuous control and robot learning using policy-gradient reinforcement learning. These methods improve planning

performance by modifying model parameters, whereas our work enforces hard constraints at inference time without retraining, making it orthogonal to training-based adaptation.

## B Stochastic optimal control and constrained sampling

We expand on Section 4 and present the connection between stochastic optimal control and safe planning with *test-time* constraints. We recall central ideas from optimal control literature [21] and motivate grounding constrained planning in this line of work.

**Stochastic Optimal Control.** For simplicity and coherence with the literature, we consider a *forward-time* Itô process between  $0 \leq t \leq 1$ , transporting probability mass from prior distribution  $p_0$  toward  $p_{base}$ . The diffusion-centric formulation in (5) is equivalent up to time reversal. We parametrize the SDE by a given reference drift  $f : \mathbb{R}^d \times [0, 1] \rightarrow \mathbb{R}^d$  and diffusion coefficient  $g : [0, 1] \rightarrow \mathbb{R}$ :

$$dX_t = f_t(X_t)dt + g(t)dW_t, \quad X_0 \sim p_0, \quad t \in [0, 1] \quad (11)$$

where  $(W_t)_{t \geq 0}$  denotes a standard Wiener process. To control generation, we introduce an additive control drift  $u : \mathbb{R}^d \times [0, 1] \rightarrow \mathcal{U}$  producing actions in the admissible set of control inputs  $\mathcal{U}$ . As optimization objectives, let  $C : \mathbb{R}^d \rightarrow \mathbb{R}$  denote the terminal cost, and  $\ell : \mathbb{R}^d \times \mathcal{U} \times [0, 1] \rightarrow \mathbb{R}$  be the running cost. Stochastic optimal control formulates the minimization problem of the expected cost functional  $J$  over the path measure  $\mathbb{P}^u$  induced by the controlled dynamics:

$$\begin{aligned} \min_{u \in \mathcal{A}} J(u) &= \mathbb{E} \left[ C(X_1^u) + \int_0^1 \ell(X_t^u, u_t(X_t^u), t) dt \right] \\ \text{s.t.} \quad dX_t^u &= [f_t(X_t^u) + g(t)u_t(X_t^u)] dt + g(t)dW_t, \\ X_0^u &\sim p_0, \quad t \in [0, 1]. \end{aligned} \quad (12)$$

where  $\mathcal{A}$  is the admissible class of progressively measurable controls satisfying  $u_t(X_t^u) \in \mathcal{U}$  and  $\mathbb{E}_{X^u \sim \mathbb{P}^u} \left[ \int_0^1 \|u_t(X_t^u)\|^2 dt \right] < \infty$ . Under standard coercivity, convexity, and continuity assumptions on the data that ensure existence of optimal controls for controlled Itô diffusions [26], we denote by  $u^* \in \arg \min_{u \in \mathcal{A}} J(u)$  an optimal solution of (12).

**Solving the SOC and the Hamilton–Jacobi–Bellman equation.** Solving (12) *as-is* is generally intractable due to the stochastic dynamics and the expectation over all realizable paths. We present a classical dynamic programming formulation that transforms the functional minimization problem into a partial differential equation (PDE). First, for a given admissible control, define the *cost-to-go*  $J : \mathcal{A} \times \mathbb{R}^d \times [0, 1] \rightarrow \mathbb{R}$  by

$$J(u; x, t) = \mathbb{E}_{\mathbb{P}_{t,x}^u} \left[ \int_t^1 \ell(X_s^u, u_s(X_s^u), s) ds + C(X_1^u) \right], \quad (13)$$

where  $\mathbb{P}_{t,x}^u$  denotes the path measure induced by the controlled dynamics initialized at  $X_t^u = x$ . The cost-to-go coincides with the expected future cost incurred by applying  $u$  from state  $x$  at time  $t$ . We then define the *value function*  $V : \mathbb{R}^d \times [0, 1] \rightarrow \mathbb{R}$  as the infimum of this cost over all admissible controls:

$$V(x, t) = \inf_{u \in \mathcal{A}} J(u; x, t). \quad (14)$$

The SOC and value formulations are related as taking expectations over the initial distribution yields:

$$J(u) = \mathbb{E}_{X_0 \sim p_0} [J(u; X_0, 0)], \quad (15)$$

$$J(u^*) = \mathbb{E}_{X_0 \sim p_0} [V(X_0, 0)]. \quad (16)$$

A solution to the stochastic optimal control problem can be achieved by computing the value function, which, under regularity conditions, satisfies the Hamilton–Jacobi–Bellman (HJB) [5] partial differential equation (Theorem 1).

**Theorem 1** (Hamilton–Jacobi–Bellman equation [21]). *Assume the standard conditions for the dynamic programming principle hold, and suppose that the value function satisfies  $V \in C^{1,2}(\mathbb{R}^d \times [0, 1])$ . Define the stochastic Hamiltonian*

$$\mathcal{H}(x, p, M, u, t) := \ell(x, u, t) + (f_t(x) + g(t)u)^\top p + \frac{1}{2}g(t)^2 \text{tr}(M). \quad (17)$$

Then  $V$  solves the Hamilton–Jacobi–Bellman equation

$$-\partial_t V(x, t) = \min_{u \in \mathcal{U}} \mathcal{H}(x, \nabla_x V(x, t), \nabla_x^2 V(x, t), u, t), \quad V(x, 1) = C(x). \quad (18)$$

Moreover, whenever the minimum is attained, an optimal feedback control satisfies

$$u^*(x, t) \in \arg \min_{u \in \mathcal{U}} \mathcal{H}(x, \nabla_x V(x, t), \nabla_x^2 V(x, t), u, t). \quad (19)$$

*Proof.* The result follows from Bellman’s dynamic programming principle [5]. Applying the principle over  $[t, t + \Delta t]$ , expanding the value function with Itô’s formula, taking expectations, and sending  $\Delta t \rightarrow 0$  leads to the differential HJB formulation. The terminal condition follows from the definition of the cost-to-go. See Fleming and Rishel [21].  $\square$

In practice, solving the HJB PDE exactly is rarely tractable beyond low-dimensional systems, because grid-based dynamic programming suffers from the curse of dimensionality; since our focus is on *training-free* guidance rather than learning value functions, we refer the reader to training-based approaches to HJB equations and stochastic optimal control, including approximate dynamic programming, reinforcement learning, and neural PDE methods [7, 24, 59, 63].

**Relation to KL control.** We now specialize the stochastic optimal control formulation by choosing the quadratic running cost

$$\ell(x, u, t) = \frac{1}{2} \|u\|^2. \quad (20)$$

This choice gives the control objective a path-space relative-entropy interpretation, connecting stochastic optimal control to Schrödinger Bridge problems, path-integral control, and KL-control as outlined in the following theorem:

**Theorem 2** (Path-space KL representation). *Let  $\{X_t^0\}_{t \in [0,1]}$  be the reference stochastic interpolant*

$$dX_t^0 = f_t(X_t^0) dt + g(t)dW_t, \quad X_0^0 \sim p_0, \quad (21)$$

*with induced path measure  $\mathbb{P}^0$ . Let  $\mathbb{P}^u$  be the path measure induced by the controlled stochastic interpolant*

$$dX_t^u = [f_t(X_t^u) + g(t)u_t(X_t^u)] dt + g(t)dW_t, \quad X_0^u \sim p_0. \quad (22)$$

*Then, for progressively measurable controls satisfying the standard Girsanov integrability condition, the SOC objective with  $\ell(x, u, t) = \frac{1}{2} \|u\|^2$  is equivalent to the KL-regularized path-space objective*

$$\inf_{u \in \mathcal{A}} \{ \text{KL}(\mathbb{P}^u \parallel \mathbb{P}^0) + \mathbb{E}_{\mathbb{P}^u} [C(X_1^u)] \}. \quad (23)$$

*Proof.* By Girsanov’s theorem, the controlled drift perturbation  $g(t)u_t$  induces an absolutely continuous change of path measure whose Radon–Nikodym derivative yields

$$\text{KL}(\mathbb{P}^u \parallel \mathbb{P}^0) = \mathbb{E}_{\mathbb{P}^u} \left[ \int_0^1 \frac{1}{2} \|u_t(X_t^u)\|^2 dt \right].$$

Substituting this identity into the SOC objective with  $\ell(x, u, t) = \frac{1}{2} \|u\|^2$  yields (23). See Theodorou and Todorov [64] for the corresponding relative-entropy derivation in path-integral and KL-control stochastic optimal control.  $\square$

Theorem 2 shows that the quadratic-control SOC objective selects a guided sampler that reduces terminal cost while remaining close to the reference stochastic interpolant in path-space KL. This principle of remaining maximally close to the reference sampler, and hence avoiding unnecessary over-constraint of the latent dynamics, offers a useful lens for safe planning with pretrained diffusion models. Although the full stochastic optimal control problem is generally intractable, we emphasize that this distributional viewpoint provides a principled idealization from which reliable and efficient training-free surrogate approximations may be derived.

**Constrained sampling.** As noted in prior work on constrained sampling [12, 71], the stochastic optimal control formulation naturally generalizes to planning with *hard* constraints. In particular, let  $\mathcal{S} \subseteq \mathbb{R}^d$  denote a feasible set and define the extended-valued indicator

$$\iota_{\mathcal{S}}(x) = \begin{cases} 0, & x \in \mathcal{S}, \\ +\infty, & x \notin \mathcal{S}. \end{cases} \quad (24)$$

Then hard-constrained sampling can be written by choosing the terminal cost  $C'(x) = C(x) + \iota_{\mathcal{S}}(x)$ , yielding the constrained SOC problem

$$\begin{aligned} \min_{u \in \mathcal{A}} \quad & \mathbb{E} \left[ \int_0^1 \frac{1}{2} \|u_t(X_t^u)\|^2 dt + C'(X_1^u) \right] \\ \text{s.t.} \quad & dX_t^u = [f_t(X_t^u) + g(t)u_t(X_t^u)] dt + g(t)dW_t, \quad X_0^u \sim p_0. \end{aligned} \quad (25)$$

Now let  $C'(x) = C(x) + \iota_{\mathcal{S}}(x)$ . Since

$$\mathbb{E}[C'(X_1)] = \mathbb{E}[C(X_1)] + \mathbb{E}[\iota_{\mathcal{S}}(X_1)],$$

any finite-cost solution must satisfy  $X_1 \in \mathcal{S}$  almost surely. Therefore, the extended-valued terminal cost is equivalently represented as an explicit terminal constraint, yielding

$$\begin{aligned} \min_{u \in \mathcal{A}} \quad & \mathbb{E}_{\mathbb{P}^u} \left[ C(X_1) + \int_0^1 \frac{1}{2} \|u_t(X_t)\|^2 dt \right] \\ \text{s.t.} \quad & dX_t^u = [f_t(X_t^u) + g(t)u_t(X_t^u)] dt + g(t)dW_t, \quad X_0^u \sim p_0 \\ & X_1 \in \mathcal{S} \quad \mathbb{P}^u\text{-a.s.} \end{aligned} \quad (26)$$

## C Algorithm derivation

In this section, we provide the full derivation of the algorithm, highlighting all the approximations employed to reach a computationally tractable formulation. For a self-contained derivation, we start by repeating the terminally constrained stochastic optimal control problem.

**Problem 1** (Continuous-time stochastic optimal control problem with terminal constraints). *Given reference dynamics, constraint set  $\mathcal{S}$ , terminal cost  $C$ , and cost weight  $\lambda$ , solve for the optimal control drift  $u^*$ :*

$$\begin{aligned} \min_u \quad & \mathbb{E} \left[ \lambda C(X_0^u) + \frac{1}{2} \int_0^1 \|u_t(X_t^u)\|_2^2 dt \right] \\ \text{s.t.} \quad & dX_t^u = [\tilde{f}_t^\theta(X_t^u) + g(t)u_t(X_t^u)] dt + g(t)d\bar{W}_t, \quad X_1 \sim p_1 \\ & X_0^u \in \mathcal{S} \quad \mathbb{P}^u\text{-a.s.} \end{aligned} \quad (27)$$

where the reverse drift is given by the learned score function  $\tilde{f}_t^\theta(X_t) = f_t(X_t) - g(t)^2 s_t^\theta(X_t)$ .

For the numerical integration of the reverse-time dynamics, let  $N \in \mathbb{N}$  denote the number of discretization steps, and let  $0 = t_0 < t_1 < \dots < t_{N-1} < t_N = 1$  be the time grid used for sampling from the diffusion model. Since diffusion sampling proceeds backward in time, we define the uncontrolled reverse update from  $t_i$  to  $t_{i-1}$  by

$$X_{i-1} = \Phi_i^\theta(X_i, \varepsilon_i), \quad i = 1, \dots, N,$$

where  $\Phi_i^\theta : \mathbb{R}^d \times \mathbb{R}^d \rightarrow \mathbb{R}^d$  is the  $i$ -th denoising transition map, and  $\varepsilon_i \sim \mathcal{N}(0, I_d)$  are independent across  $i$ . The maps  $\Phi_i^\theta$  are left abstract in order to accommodate different numerical sampling schemes. Moreover, as is commonly done to reduce discretization-induced noise in the final sample, we assume that the last denoising step is deterministic and returns the model's data prediction without injecting additional noise. That is,

$$X_0 = \Phi_1^\theta(X_1) = \hat{x}_0^\theta(X_1, t_1).$$

For the SOC surrogate, we approximate the controlled dynamics by applying an Euler discretization to the control input over each interval  $[t_{i-1}, t_i]$ . This yields

$$X_{i-1}^u = \Phi_i^\theta(X_i^u, \varepsilon_i) + g_i u_i(X_i^u) \Delta t_i, \quad i = 1, \dots, N, \quad (28)$$

where  $g_i = g(t_i)$ ,  $\Delta t_i = t_i - t_{i-1}$ , and  $\varepsilon_i \sim \mathcal{N}(0, I_d)$ . After discretizing the control energy, we obtain the discrete-time formulation of the terminally constrained stochastic optimal control problem, stated in Problem 2.

**Problem 2** (Discrete-time stochastic optimal control problem with terminal constraints). *Given reference drift  $f_t^\theta$ , constraint set  $\mathcal{S}$ , and cost weight  $\lambda$ , solve for the control functions  $\{u_i^*\}_{i=1}^N$ :*

$$\begin{aligned} \min_{\{u_i\}_{i=1}^N} \quad & \mathbb{E} \left[ \lambda C(X_0^u) + \frac{1}{2} \sum_{i=1}^N \|u_i(X_i^u)\|_2^2 \Delta t_i \right] \\ \text{s.t.} \quad & X_{i-1}^u = \Phi_i^\theta(X_i^u, \varepsilon_i) + g_i u_i(X_i^u) \Delta t_i, \quad \varepsilon_i \sim \mathcal{N}(0, I_d), \quad \forall i, 1 \leq i \leq N, \\ & X_0^u \in \mathcal{S} \quad \mathbb{P}_d^u\text{-a.s.} \end{aligned} \quad (29)$$

where  $\mathbb{P}_d^u$  is the probability measure over state tuples induced by the controlled dynamics.

Although the preceding discretization yields a finite-horizon control problem, the optimization problem remains largely intractable in its full generality. First, the control variables are defined over the full state space  $\mathbb{R}^d$ , while the objective involves an expectation over all realizations of the controlled stochastic dynamics. Moreover, terminal costs and hard terminal constraints induce temporal coupling across the full reverse process: the effect of an early control perturbation on the terminal state is mediated by a long composition of neural-network denoising maps.

Rearranging the controlled dynamics, we can express the control action at each step in terms of the deviation from the uncontrolled denoising update.<sup>1</sup> Namely,

$$u_i = \frac{X_{i-1} - \bar{X}_{i-1}^{\varepsilon_i}}{g_i \Delta t_i}, \quad \bar{X}_{i-1}^{\varepsilon_i} := \Phi_i^\theta(X_i, \varepsilon_i), \quad i = 1, \dots, N. \quad (30)$$

Second, motivated by model predictive control [52], we replace the full-horizon optimization by a one-step look-ahead surrogate. Specifically, at step  $i$ , the transition from  $X_i$  to  $X_{i-1}$  is evaluated using the original denoising update, while the cost-to-go over the remaining reverse process is approximated using the model's predicted clean sample. This yields the proxy

$$\mathbb{E}[C(X_0) \mid X_{i-1}] \approx C(\mathbb{E}[X_0 \mid X_{i-1}]) \approx C(\hat{x}_0^\theta(X_{i-1}, t_{i-1})), \quad i = 1, \dots, N. \quad (31)$$

The total discrete-time SOC cost-to-go from step  $i$  is therefore approximated by retaining only the one-step control effort and replacing the remaining terminal cost by the Tweedie-based prediction. Namely, we use the surrogate

$$\mathbb{E} \left[ \lambda C(X_0) + \frac{1}{2} \sum_{k=1}^i \|u_k(X_k)\|_2^2 \Delta t_k \mid X_i \right] \approx \lambda C(\hat{x}_0^\theta(X_{i-1}, t_{i-1})) + \frac{1}{2g_i^2 \Delta t_i} \|X_{i-1} - \bar{X}_{i-1}^{\varepsilon_i}\|_2^2. \quad (32)$$

Similarly, we enforce constraint satisfaction on the predicted clean sample  $\hat{x}_0^\theta(X_{i-1}, t_{i-1})$  as a proxy for terminal feasibility, thereby replacing the full joint optimization over all control variables with a sequence of one-step subproblems. At each denoising step, we first compute  $\bar{X}_{i-1}^{\varepsilon_i} = \Phi_i^\theta(X_i, \varepsilon_i)$ , with  $\varepsilon_i \sim \mathcal{N}(0, I_d)$ , and correct the uncontrolled estimate by solving:

$$\begin{aligned} X_{i-1}^* \in \arg \min_{X_{i-1}} \quad & \lambda C(\hat{X}_{0|i-1}) + \frac{1}{2g_i^2 \Delta t_i} \|X_{i-1} - \bar{X}_{i-1}^{\varepsilon_i}\|_2^2 \\ \text{s.t.} \quad & \hat{X}_{0|i-1} \in \mathcal{S}, \quad \hat{X}_{0|i-1} = \hat{x}_0^\theta(X_{i-1}, t_{i-1}). \end{aligned} \quad (33)$$

Each one-step subproblem still contains a nontrivial coupling between the optimization variable  $X_{i-1}$  and the predicted clean sample  $\hat{X}_{0|i-1} := \hat{x}_0^\theta(X_{i-1}, t_{i-1})$ . This coupling enters both the terminal cost and the feasibility constraint  $\hat{X}_{0|i-1} \in \mathcal{S}$ . Therefore, even when  $C$  and  $\mathcal{S}$  have simple structure in the data domain, their pullback through the neural denoising map  $\hat{x}_0^\theta(\cdot, t_{i-1})$  may define a highly nonlinear and nonconvex optimization problem in the latent variable  $X_{i-1}$ . For diffusion policies with tentatively millions of parameters, repeatedly embedding neural-network evaluations within the

<sup>1</sup>We also simplify the notation and suppress the superscript  $u$  and write  $X_i$  instead of  $X_i^u$  for controlled states.

subproblem can introduce substantial computational overhead and may limit the practicality of direct latent-space optimization with generic off-the-shelf solvers. To phrase the optimization in the data domain, we approximate the latent displacement  $X_{i-1} - \bar{X}_{i-1}^{\varepsilon_i}$  through the corresponding difference between predicted clean samples. The key step is to approximately invert Tweedie’s formula by a fixed-point scheme. Rearranging (3) at time  $t_{i-1}$  gives

$$X_{i-1} = \alpha_{t_{i-1}} \hat{x}_0^\theta(X_{i-1}, t_{i-1}) - \sigma_{t_{i-1}}^2 s_{t_{i-1}}^\theta(X_{i-1}). \quad (34)$$

Now fix  $y = \hat{x}_0^\theta(X_{i-1}, t_{i-1})$ . Inverting Tweedie’s estimate for this prescribed clean prediction amounts to finding  $X_{i-1}$  such that

$$X_{i-1} = F_{t_{i-1}}^\theta(X_{i-1}; y), \quad F_{t_{i-1}}^\theta(x; y) := \alpha_{t_{i-1}} y - \sigma_{t_{i-1}}^2 s_{t_{i-1}}^\theta(x). \quad (35)$$

Assuming  $F_{t_{i-1}}^\theta(\cdot; y)$  is a contraction, the Banach fixed-point theorem guarantees a unique fixed point, which can be obtained by repeated application of  $F_{t_{i-1}}^\theta(\cdot; y)$ :

$$X_{t_{i-1}}^*(y) = \lim_{k \rightarrow \infty} \left( F_{t_{i-1}}^\theta(\cdot; y) \right)^{(k)} (X^{(0)}). \quad (36)$$

In practice, we initialize the fixed-point inversion at the uncontrolled proposal  $\bar{X}_{i-1}^{\varepsilon_i}$ , which provides a natural estimate of the latent state before control is applied. Applying one fixed-point iteration gives

$$X_{i-1} \approx F_{t_{i-1}}^\theta(\bar{X}_{i-1}^{\varepsilon_i}; y) = \alpha_{t_{i-1}} y - \sigma_{t_{i-1}}^2 s_{t_{i-1}}^\theta(\bar{X}_{i-1}^{\varepsilon_i}). \quad (37)$$

Combining this approximation with (34) applied to  $\bar{X}_{i-1}^{\varepsilon_i}$  yields

$$\begin{aligned} X_{i-1} - \bar{X}_{i-1}^{\varepsilon_i} &\approx \alpha_{t_{i-1}} (y - \hat{x}_0^\theta(\bar{X}_{i-1}^{\varepsilon_i}, t_{i-1})) \\ &= \alpha_{t_{i-1}} (\hat{x}_0^\theta(X_{i-1}, t_{i-1}) - \hat{x}_0^\theta(\bar{X}_{i-1}^{\varepsilon_i}, t_{i-1})). \end{aligned} \quad (38)$$

Thus, the latent displacement can be approximated by a scaled discrepancy between Tweedie clean-sample predictions. This provides a gradient-free correction direction in latent space and allows the control penalty to be expressed in the data domain. Substituting (38) into the one-step surrogate yields the final receding-horizon formulation in Problem 3, where the constrained optimization is carried out in the data domain rather than through repeated neural-network evaluations inside the solver.

**Problem 3** (DiRecT: receding-horizon formulation). *Given a sampling scheme  $\{\Phi_i^\theta\}_{i=1}^N$ , constraint set  $\mathcal{S}$ , cost weight  $\lambda$ , and initial sample  $X_N^* \sim p_{\text{prior}}$ , solve the following recursion for  $i = N, \dots, 1$ :*

$$\begin{cases} \bar{X}_{i-1}^{\varepsilon_i} = \Phi_i^\theta(X_i^*, \varepsilon_i), & \varepsilon_i \sim \mathcal{N}(0, I_d), \\ \tilde{X}_{0|i-1} = \hat{x}_0^\theta(\bar{X}_{i-1}^{\varepsilon_i}, t_{i-1}), \\ \hat{X}_{0|i-1}^* \in \arg \min_{\hat{X}_{0|i-1}} \lambda C(\hat{X}_{0|i-1}) + \frac{\alpha_{t_{i-1}}^2}{2g_i^2 \Delta t_i} \|\hat{X}_{0|i-1} - \tilde{X}_{0|i-1}\|_2^2 & \text{s.t. } \hat{X}_{0|i-1} \in \mathcal{S}, \\ X_{i-1}^* = \begin{cases} \bar{X}_{i-1}^{\varepsilon_i} + \alpha_{t_{i-1}} (\hat{X}_{0|i-1}^* - \tilde{X}_{0|i-1}), & i > 1, \\ \hat{X}_{0|0}^*, & i = 1. \end{cases} \end{cases} \quad (39)$$

Although several approximations are introduced to reduce the general stochastic optimal control problem to a tractable form, terminal constraint satisfaction is not relaxed, as formalized in Proposition 1.

**Remark 1** (Terminal convention). *At the final denoising step, we return the optimized data-domain prediction  $\hat{X}_{0|0}^*$  directly, rather than applying the latent correction formula. This convention ensures exact terminal feasibility whenever the final subproblem is solved feasibly. It is also convenient in practical implementations, since common noise schedules, such as cosine schedules [47], need not satisfy  $\alpha_{t_0} = 1$  exactly.*

## D Implementation details

**Hardware.** All Maze2D and D3IL experiments were performed on a compute node equipped with two Intel(R) Xeon(R) Gold 5218 @ 2.30GHz CPUs and six NVIDIA Quadro RTX 8000 48GB, MRMP

on a node with two Intel Xeon E5-2670 v2 @ 2.50 GHz CPUs and one NVIDIA Tesla V100-SXM2 32 GB GPU, and PushT on a machine equipped with two AMD EPYC 75F3 32-Core Processor CPUs and four NVIDIA A100 GPUs. All computations for training, model evaluation, and gradient calculation were performed on a single GPU, whereas environment rollouts and IPOPT optimizations were performed on a CPU.

**Software.** All experiments are based on PyTorch [49] for automatic differentiation and JAX [11] for our custom multi-agent path-finding optimizer. Moreover, MRMP and PushT are based on PROJECTED COUPLED DIFFUSION [43]<sup>2</sup> (MIT), which are themselves extensions of DIFFUSION POLICY [13]<sup>3</sup> (MIT), MMD [58]<sup>4</sup> (MIT), and LTLDOG [20]<sup>5</sup> (MIT). We use CASADi [4] (GNU LGPL v3.0) and IPOPT [68] (EPL-2.0) for *off-the-shelf* optimization.

## D.1 Safe maze navigation

**Training.** We train a *continuous-time* diffusion model with a standard temporal UNet architecture [30] and horizon  $H = 384$ . The model outputs the state-action pair trajectory  $(s_0, a_0, s_1, a_1, \dots, s_{H-1}, a_{H-1}) \in \mathbb{R}^{6H}$  conditioned on given start and end states. We employ data-prediction parametrization and a cosine noise schedule with offset  $s = 0.008$  [47]. We train the model with Adam [34] for 500,000 steps with a batch size of 256 on the D4RL maze2d-large-v1 [23]<sup>6</sup> dataset (CC BY 4.0), scaled by min-max normalization. We use a learning rate of 0.001 with a cosine annealing schedule for the first 10,000 steps. We save checkpoints using an exponential moving average of the model weights with decay 0.995.

**Environment details.** We introduce obstacles as ellipses and super-ellipses centered in  $(c_x, c_y)$ , semi-axes  $(r_x, r_y)$ , and order  $p$ :

$$\left| \frac{x - c_x}{r_x} \right|^p + \left| \frac{y - c_y}{r_y} \right|^p \geq 1 \quad (40)$$

For both Broad and Narrow variants, we follow the obstacle placement in [69]. To enforce dynamics constraints we fit by ordinary least-squares regression the normalized transitions from the training data for a total of 3,993,503 across 1,062 episodes. For simplicity, although equivalent, we separate the state and action coefficients with the following functional form  $s' = A \cdot s + B \cdot a + c$ , where each transition is defined by the tuple  $(s, a, s')$ . When enforcing dynamic constraints, we impose the fitted dynamics as *strict* equality constraints over the planning horizon. Although the per-step least squares residuals are contained, open-loop execution over the full horizon remains impractical. In this regime, predicted and executed trajectories may diverge, hindering proper evaluation of the planner. To mitigate this issue, we perform policy rollout by tracking the generated trajectory with a proportional-derivative (PD) controller with constants  $P = 5, D = 1$ .

**Evaluation.** We evaluate each method over 100 i.i.d. generated samples conditioned on the same fixed endpoints. For each sample, we execute a rollout up to 800 environment steps, at which the episode is terminated. For all methods we denoise with a DDPM sampler [28] on a uniform time discretization. We follow standard practice and perform the last denoising iteration by returning the model prediction. To encourage shorter paths, when applicable, the cost function  $C(x)$  is chosen to be the squared path length of the generated trajectory. We now briefly describe the implementation details of each method, as well as their adaptation to include equality dynamic constraints:

- **Diffuser** [29]. We employ 32 denoising iterations as an unguided reference for the base pretrained model. No obstacles or dynamic constraints are imposed.
- **Gradient Guidance** [15]. We employ 32 denoising iterations and guide the noisy latent  $x_t$  by computing the gradient of the cost function using posterior sampling as  $\nabla C'(\hat{x}_{0,\theta}(x_t))$ , where constraint violations are added as a penalty term in the cost function  $C'(x) = C(x) + C_{\text{penalty}}(x)$ . To impose dynamic constraints, we penalize the squared residuals of

<sup>2</sup><https://github.com/EdmundLuan/pcd>

<sup>3</sup>[https://github.com/real-stanford/diffusion\\_policy](https://github.com/real-stanford/diffusion_policy)

<sup>4</sup><https://github.com/yoraish/mmd>

<sup>5</sup><https://github.com/clear-nus/ltldog>

<sup>6</sup><https://github.com/Farama-Foundation/D4RL>

each predicted transition along the prediction horizon by adding them as an additional cost penalty.

- **Projection** [14]. We employ 32 denoising steps and project the second half of the generated latents onto the feasible set. Dynamic constraints are introduced directly in the optimization process, which is solved with IPOPT.
- **Augmented Lagrangian** [71]. We adapt the original implementation to the continuous-time case by scaling hyperparameters to generate equivalent guided transitions. We use 256 sampling steps with an additional 200 iterations for the last denoising step. We use the original implementation for handling dynamic equality constraints.
- **SafeDiffuser-RoS** [69]. We adapt the original implementation to the continuous-time case by scaling hyperparameters to generate equivalent guided transitions with 256 sampling steps. We introduce dynamic constraints directly into the quadratic program. The resulting optimization problem is solved with IPOPT.
- **DiRecT**. We employ 32 denoising steps and optimize over the second half of the generative process. We incorporate dynamic constraints directly into the receding-horizon subproblem, which is solved with IPOPT.

## D.2 Safe robotic manipulation

We train a *continuous-time* diffusion model with a temporal UNet architecture [30] and horizon  $H = 16$ . The model outputs the state-action pair trajectory  $(s_0, a_0, s_1, a_1, \dots, s_{H-1}, a_{H-1}) \in \mathbb{R}^{6H}$  over the entire prediction horizon. We employ data-prediction parametrization and a cosine noise schedule with offset  $s = 0.008$  [47]. We train the model with Adam [34] for 500,000 steps with a batch size of 32 on the D3IL avoiding dataset [30]<sup>7</sup> (MIT), scaled by min-max normalization. We use a learning rate of  $2 \times 10^{-4}$  with a cosine annealing schedule for the first 100,000 steps. We save checkpoints using an exponential moving average of the model weights with decay 0.995.

**Environment details.** The base D3IL avoiding task presents six circular pillars that must be avoided by the end-effector. The unguided diffusion policy learns to dodge these obstacles directly from human demonstrations. To assess performance over *unseen* constraints, we restrict planning by increasing the radius of the first pillar and limiting side-movements by two planar regions. Dynamics constraints are imposed by least-squares fitting of the 7209 training transitions across 96 demonstrations, with the same procedure for Maze2D (see Appendix D.1).

**Evaluation.** We evaluate each method over 100 i.i.d. generated samples conditioned on a fixed initial position and with zero starting velocity. For each sample, we execute a rollout up to 100 environment steps with a planning horizon  $H = 16$  and execution horizon  $M = 4$ . We terminate the episode when the end-effector collides with a pillar, while we continue rollouts for violations of *test-time* constraints. All other implementation details follow the procedure for Maze2D (see Appendix D.1).

## D.3 Safe multi-robot motion planning

**Problem setup.** In this task, multiple agents’ trajectories in a common environment are generated in a collision-free and velocity-constrained manner. We test our method on the four environments from the MMD [58] benchmark. A diffusion model is trained for each environment on single-agent trajectories showing a specific motion pattern. In the unconstrained setting, the objective is to generate trajectories  $\tau \in \mathbb{R}^{H \times 2}$  conditioned on given start and target endpoints  $(b, e) \in \mathbb{R}^{2 \times 2}$  presenting the desired motion behaviors for each MMD environment (Figure 5):

- **Empty** is the simplest map, where demonstrations consist of straight-line motions and robots are penalized for deviating from a direct path.
- **Highways** contains a central block that induces a warehouse-like traffic pattern, where agents are expected to move *counterclockwise* around the obstacle.
- **Conveyor** consists of two narrow corridors. Agents are rewarded for moving leftward in the top corridor and rightward in the bottom corridor.

<sup>7</sup><https://github.com/ALRhub/d3il>

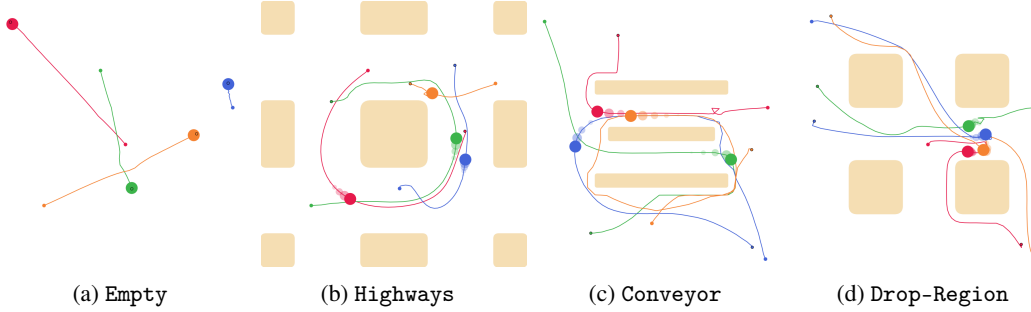


Figure 5: Four major MMD environments with feasible optimized solutions. Robots navigate toward their goal positions while avoiding inter-robot and obstacle collisions and satisfying velocity constraints. Each environment exhibits a characteristic motion pattern that should be preserved.

- Drop-Region features an obstacle-free central space and four drop-off regions. Agents are rewarded for pausing near the midpoint of any of the four square regions, emulating package-delivery tasks.

Following the coupled trajectory-generation setup in [43], we seek to generate  $N_a$  agent trajectories *simultaneously*. The generated trajectories must avoid inter-robot and robot-obstacle collisions, satisfy *test-time* velocity restrictions, and exhibit the desired MMD motion pattern.

Let  $[K]$  denote  $\{1, \dots, K\}$  for any natural number  $K \in \mathbb{N}$ . We denote a generated sample of trajectories by  $\tau = (\tau_1, \dots, \tau_{N_a}) \in \mathbb{R}^{N_a \times H \times 2}$ , where  $\tau_i^j$  is the  $j$ -th predicted step for the  $i$ -th agent. Given an optimization objective  $\mathcal{J} : \mathbb{R}^{N_a \times H \times 2} \rightarrow \mathbb{R}$  and starting locations  $\{b_i\}_{i \in [N_a]}$  for each robot, the general MRMP problem is formulated as [39, 58]

$$\min_{\tau \in \mathbb{R}^{N_a \times H \times 2}} \mathcal{J}(\tau) \quad (41a)$$

$$\text{s.t.} \quad \|\tau_i^{k+1} - \tau_i^k\|_2 \leq v_{\max} \Delta t, \quad \forall i \in [N_a], \forall k \in [H-1], \quad (41b)$$

$$\|\tau_i^1 - b_i\|_2 \leq v_{\max} \Delta t, \quad \forall i \in [N_a], \quad (41c)$$

$$\|\tau_i^k - \tau_j^k\|_2 \geq 2\delta, \quad \forall i \neq j, \forall k \in [H], \quad (41d)$$

$$d(\tau_i^k, \mathcal{O}) \geq \delta, \quad \forall i \in [N_a], \forall k \in [H]. \quad (41e)$$

where  $\delta$  is the robot radius,  $v_{\max}$  is the test-time maximum allowable velocity,  $\Delta t$  is the environment time increment between consecutive generated steps, and  $d(\cdot, \mathcal{O}) : \mathbb{R}^2 \rightarrow \mathbb{R}$  is the distance function to the obstacle set. Let  $\Omega_V$ ,  $\Omega_{CR}$ , and  $\Omega_{CO}$  denote the feasible sets associated with the velocity, inter-robot collision-avoidance, and robot-obstacle collision-avoidance constraints, respectively. We define the feasible set of Problem 41 as  $\Omega = \Omega_V \cap \Omega_{CR} \cap \Omega_{CO}$ . The data adherence objective is implicitly specified by the single-agent diffusion policy. In this setting, Problem 41 can be naturally interpreted as constrained sampling from a pretrained diffusion model applied to the concatenation of all agent trajectories. More explicitly, given a diffusion model trained for a single agent, we can generate  $N_a$  independent trajectories by sampling from the product distribution

$$\tau \sim p_0^*(\tau) = \prod_{i=1}^{N_a} p_0(\tau_i).$$

Therefore, the corresponding concatenated denoiser  $\hat{x}_{0,\theta}^*(\tau) = \bigoplus_{i=1}^{N_a} \hat{x}_{0,\theta}(\tau_i)$  is equivalent to a pretrained diffusion model that interpolates between the prior  $\mathcal{N}(0, \mathbf{I}_{N_a \times H \times 2})$  and the product distribution  $p_0^*$ . To impose *test-time* constraints within our framework, we define a *projection* operator onto the feasible set  $\Omega$ . This differs from the coupled diffusion framework of [43] where only velocity limits are enforced exactly: rather than relying on soft collision penalties, we impose the nonconvex collision-avoidance constraints as hard constraints in the constrained optimization problem.

**Evaluation details.** We use the pretrained checkpoints provided by [43], which are trained with a Diffusion Policy [13] backbone on the four MMD environments. For each environment, we

impose a maximum allowable agent velocity, computed from forward differences of trajectory positions. For all methods, we generate samples using 100 DDPM [28] denoising steps, applying guidance during the second half of the denoising process. We evaluate each method over 100 randomly selected initial configurations. For each configuration, we generate a batch of 128 candidate trajectories in parallel. Following [43], we define *Success Rate* as the fraction of trials for which at least one trajectory in the generated batch is collision-free. In contrast, *Constraint Safety* measures the average feasibility rate over *all* generated trajectories in terms of both collision and kinematic constraints.

### D.3.1 Custom MRMP optimizer

**Problem setup.** We explicitly state the projection problem solved by the MRMP optimizer. Let  $X \in \mathbb{R}^{N_a \times H \times 2}$  denote the optimized trajectory tuple, with  $X_i^k \in \mathbb{R}^2$  denoting the position of agent  $i$  at waypoint  $k$ . Let  $\hat{X} \in \mathbb{R}^{N_a \times H \times 2}$  denote the Tweedie clean-trajectory estimate produced by the diffusion model. The proximal safe trajectory is computed as the solution of

$$X^* = \arg \min_{X \in \mathbb{R}^{N_a \times H \times 2}} \frac{1}{2} \|X - \hat{X}\|_F^2 + \frac{\lambda_{\text{sm}}}{2} \sum_{i=1}^{N_a} \sum_{k=1}^{H-1} \|X_i^{k+1} - X_i^k\|_2^2. \quad (42a)$$

$$\text{s.t.} \quad \|X_i^1 - b_i\|_2 \leq v_{\text{max}} \Delta t, \quad \forall i \in [N_a], \quad (42b)$$

$$\|X_i^{k+1} - X_i^k\|_2 \leq v_{\text{max}} \Delta t, \quad \forall i \in [N_a], \forall k \in [H-1], \quad (42c)$$

$$\|X_i^k - X_j^k\|_2 \geq 2\delta, \quad \forall i \neq j, \forall k \in [H], \quad (42d)$$

$$d(X_i^k, \mathcal{O}) \geq \delta, \quad \forall i \in [N_a], \forall k \in [H]. \quad (42e)$$

The first term keeps the projected tuple close to the diffusion model’s Tweedie estimate  $\hat{X}$ , while the smoothness term with strength  $\lambda_{\text{sm}}$  optionally encourages straight-line trajectories. The constraints enforce initial-state consistency, inference-time velocity limits, inter-robot separation, and robot-obstacle clearance. Thus, the optimizer defines a (proximal) projection  $X^* = \Pi_{\Omega}(\hat{X})$  onto the feasible set  $\Omega = \Omega_V \cap \Omega_{CR} \cap \Omega_{CO}$ .

Different approaches are possible for solving this problem. A first possibility is to employ an off-the-shelf nonlinear solver such as IPOPT. However, general-purpose nonlinear solvers are typically designed around CPU-based sparse linear algebra and do not provide a plug-and-play GPU implementation suitable for extensive sweeps and batched inference. An alternative is to relax the nonconvex collision constraints and optimize the resulting objective with Lagrangian or augmented-Lagrangian methods [39]. However, since the collision constraints enter the objective through nonlinear penalty or multiplier terms, the resulting optimization can remain nonconvex and still requires a general-purpose CPU-based nonlinear solver. Inspired by the ADMM projector in [43], given the convexity of the velocity constraints and the spatially local structure of the collision constraints, we derive a custom optimizer by combining successive convexification of the active collision constraints with an ADMM splitting of the resulting convex subproblem [10, 44]. The complete derivation is as follows.

**Successive convexification.** The nonconvexity of (42) arises from the inter-robot and robot-obstacle collision constraints. We handle these constraints with an outer successive-convexification loop. Let  $X^{(m)}$  denote the current trajectory at SCP iteration  $m$ . For each active inter-robot constraint, define

$$r_{ij}^{k,(m)} = X_i^{k,(m)} - X_j^{k,(m)}, \quad n_{ij}^{k,(m)} = \frac{r_{ij}^{k,(m)}}{\|r_{ij}^{k,(m)}\|_2}.$$

Using the first-order lower approximation of the norm, we replace  $\|X_i^k - X_j^k\|_2 \geq 2\delta$  with

$$(n_{ij}^{k,(m)})^\top (X_i^k - X_j^k) \geq 2\delta.$$

For robot-obstacle constraints, let  $d_\ell(p)$  denote the signed distance from point  $p$  to obstacle primitive  $\mathcal{O}_\ell$ . For each active constraint  $d_\ell(X_i^k) - \delta \geq 0$ , we use the first-order approximation around  $X_i^{k,(m)}$ :

$$d_\ell(X_i^{k,(m)}) - \delta + \nabla d_\ell(X_i^{k,(m)})^\top (X_i^k - X_i^{k,(m)}) \geq 0.$$

For all MMD environments, obstacles decompose into rectangular and circular primitives, so both signed distances and their gradients can be computed exactly. At SCP iteration  $m$ , we compute the next trajectory  $X^{(m+1)}$  by solving the following convexified, slack-penalized projection problem:

$$(X^{(m+1)}, s^{(m+1)}) \in \arg \min_{X, s} \frac{1}{2} \|X - \hat{X}\|_F^2 + \frac{\lambda_{\text{sm}}}{2} \sum_{i=1}^{N_a} \sum_{k=1}^{H-1} \|X_i^{k+1} - X_i^k\|_2^2 + \frac{\tau_m}{2} \|X - X^{(m)}\|_F^2 + \mu_m \mathbf{1}^\top s. \quad (43a)$$

$$\text{s.t. } \|X_i^1 - b_i\|_2 \leq v_{\max} \Delta t, \quad \forall i \in [N_a], \quad (43b)$$

$$\|X_i^{k+1} - X_i^k\|_2 \leq v_{\max} \Delta t, \quad i \in [N_a], k \in [H-1], \quad (43c)$$

$$(n_{ij}^{k,(m)})^\top (X_i^k - X_j^k) + s_{ij}^k \geq 2\delta, \quad \forall (i, j, k) \in \mathcal{A}_{\text{RR}}^{(m)}, \quad (43d)$$

$$(n_{i\ell}^{k,(m)})^\top X_i^k + s_{i\ell}^k \geq (n_{i\ell}^{k,(m)})^\top X_i^{k,(m)} - (d_\ell(X_i^{k,(m)}) - \delta), \quad \forall (i, \ell, k) \in \mathcal{A}_{\text{O}}^{(m)}, \quad (43e)$$

$$s \geq 0. \quad (43f)$$

Here  $\mathcal{A}_{\text{RR}}^{(m)}$  and  $\mathcal{A}_{\text{O}}^{(m)}$  denote the active inter-robot and robot-obstacle constraints at the linearization point  $X^{(m)}$ . The slack variables  $s \geq 0$  keep the convexified subproblem feasible, while the  $\ell_1$  penalty  $\mathbf{1}^\top s = \|s\|_1$  encourages sparse violations. We use monotone schedules  $\mu_{m+1} = \min\{\gamma_\mu \mu_m, \mu_{\max}\}$  and  $\tau_{m+1} = \min\{\gamma_\tau \tau_m, \tau_{\max}\}$ , with  $\gamma_\mu, \gamma_\tau > 1$ . Increasing  $\mu_m$  progressively enforces collision satisfaction, while increasing  $\tau_m$  regularizes each SCP step around its linearization point.

**ADMM splitting.** To solve (43), we introduce auxiliary variables  $V, C, Z \in \mathbb{R}^{N_a \times H \times 2}$ . The variable  $V$  is used to impose velocity feasibility,  $Z$  stores the corresponding velocity increments, and  $C$  isolates the linearized collision constraints. For notational convenience, set  $V_i^0 = b_i$  and define the anchored first-difference operator

$$(D_b V)_i^k = V_i^k - V_i^{k-1}, \quad i \in [N_a], k \in [H].$$

Thus,  $(D_b V)_i^1 = V_i^1 - b_i$  encodes the initial velocity constraint, while the remaining entries encode consecutive displacements. The velocity constraint is equivalently written as  $D_b V = Z$ ,  $Z \in \mathcal{K}_Z$  with

$$\mathcal{K}_Z = \{Z : \|Z_i^k\|_2 \leq v_{\max} \Delta t, i \in [N_a], k \in [H]\}.$$

Let  $G^{(m)}$  denote the matrix collecting the active linearized collision constraints at SCP iteration  $m$ , and let  $h^{(m)}$  denote the corresponding vector of right-hand sides. The slack variable  $s$  has the same dimension as  $h^{(m)}$  and keeps the active collision constraints feasible. We write these constraints compactly as  $(C, s) \in \mathcal{K}_C^{(m)}$ , where

$$\mathcal{K}_C^{(m)} = \{(C, s) : G^{(m)} C + s \geq h^{(m)}, s \geq 0\}.$$

Let  $\mathbb{I}_{\mathcal{K}}$  denote the indicator function of a set  $\mathcal{K}$ , equal to 0 on  $\mathcal{K}$  and  $+\infty$  otherwise. Define

$$f_m(X) = \frac{1}{2} \|X - \hat{X}\|_F^2 + \frac{\lambda_{\text{sm}}}{2} \sum_{i=1}^{N_a} \sum_{k=1}^{H-1} \|X_i^{k+1} - X_i^k\|_2^2 + \frac{\tau_m}{2} \|X - X^{(m)}\|_F^2.$$

The SCP subproblem can then be written in ADMM form as

$$\begin{aligned} \min_{X, V, C, Z, s} \quad & f_m(X) + \mu_m \mathbf{1}^\top s + \mathbb{I}_{\mathcal{K}_Z}(Z) + \mathbb{I}_{\mathcal{K}_C^{(m)}}(C, s) \\ \text{s.t.} \quad & X = V, \quad X = C, \quad D_b V = Z, \quad s \geq 0. \end{aligned} \quad (44)$$

Using scaled dual variables  $U_{XV}$ ,  $U_{XC}$ , and  $U_Z$  with penalties  $\rho_{XV}$ ,  $\rho_{XC}$ ,  $\rho_Z > 0$ , the corresponding scaled augmented Lagrangian formulation of (44) is:

$$\begin{aligned} \mathcal{L}_\rho = & f_m(X) + \mu_m \mathbf{1}^\top s + \mathbb{I}_{\mathcal{K}_Z}(Z) + \mathbb{I}_{\mathcal{K}_C^{(m)}}(C, s) \\ & + \frac{\rho_{XV}}{2} \|X - V + U_{XV}\|_F^2 - \frac{\rho_{XV}}{2} \|U_{XV}\|_F^2 \\ & + \frac{\rho_{XC}}{2} \|X - C + U_{XC}\|_F^2 - \frac{\rho_{XC}}{2} \|U_{XC}\|_F^2 \\ & + \frac{\rho_Z}{2} \|D_b V - Z + U_Z\|_F^2 - \frac{\rho_Z}{2} \|U_Z\|_F^2. \end{aligned} \quad (45)$$

ADMM then alternates between the following updates at inner iteration  $q$  of SCP iteration  $m$ . For the linear solves, write the anchored difference as  $D_b V = AV - B$ , where  $A$  is the first-difference matrix with  $(AV)_i^1 = V_i^1$  and  $(AV)_i^k = V_i^k - V_i^{k-1}$  for  $k \geq 2$ , while  $B_i^1 = b_i$  and  $B_i^k = 0$  for  $k \geq 2$ .

- **$X$ -update.** The  $X$ -update minimizes the scaled augmented Lagrangian with respect to  $X$  while keeping the remaining variables fixed:

$$X^{q+1} = \arg \min_X \left\{ f_m(X) + \frac{\rho_{XV}}{2} \|X - V^q + U_{XV}^q\|_F^2 + \frac{\rho_{XC}}{2} \|X - C^q + U_{XC}^q\|_F^2 \right\}.$$

This is an unconstrained quadratic program. Setting its gradient to zero gives the linear system

$$\left( (1 + \tau_m + \rho_{XV} + \rho_{XC})I + \lambda_{\text{sm}} D^\top D \right) X^{q+1} = \hat{X} + \tau_m X^{(m)} + \rho_{XV}(V^q - U_{XV}^q) + \rho_{XC}(C^q - U_{XC}^q),$$

where  $D$  is the unanchored first-difference operator appearing in the smoothness term.

- **$V$ -update.** The  $V$ -update collects the terms involving the velocity split:

$$V^{q+1} = \arg \min_V \left\{ \frac{\rho_{XV}}{2} \|X^{q+1} - V + U_{XV}^q\|_F^2 + \frac{\rho_Z}{2} \|D_b V - Z^q + U_Z^q\|_F^2 \right\}.$$

This is also an unconstrained quadratic program. Using  $D_b V = AV - B$ , its optimality condition yields

$$(\rho_{XV}I + \rho_Z A^\top A) V^{q+1} = \rho_{XV}(X^{q+1} + U_{XV}^q) + \rho_Z A^\top (Z^q - U_Z^q + B).$$

- **$Z$ -update.** The  $Z$ -update enforces the velocity bound by projecting the current anchored displacement estimate onto  $\mathcal{K}_Z$ :

$$Z^{q+1} = \Pi_{\mathcal{K}_Z}(D_b V^{q+1} + U_Z^q).$$

This projection has a closed-form solution as it is applied *row-wise*. For  $\nu_i^k = (D_b V^{q+1})_i^k + (U_Z^q)_i^k$ ,

$$Z_i^{k,q+1} = \begin{cases} (v_{\max} \Delta t) \frac{\nu_i^k}{\|\nu_i^k\|_2}, & \|\nu_i^k\|_2 > v_{\max} \Delta t, \\ \nu_i^k, & \text{otherwise,} \end{cases} \quad i \in [N_a], k \in [H].$$

- **$C, s$ -update.** The collision update projects onto the linearized collision constraints while penalizing slack:

$$(C^{q+1}, s^{q+1}) = \arg \min_{(C,s) \in \mathcal{K}_C^{(m)}} \left\{ \frac{\rho_{XC}}{2} \|C - (X^{q+1} + U_{XC}^q)\|_F^2 + \mu_m \mathbf{1}^\top s \right\}.$$

This is a convex quadratic program with linear inequality constraints. Rather than calling a generic QP solver, we solve its box-constrained dual. Let  $Q^q = X^{q+1} + U_{XC}^q$ . The dual problem is

$$\lambda^* = \arg \max_{0 \leq \lambda \leq \mu_m} \left\{ -\frac{1}{2\rho_{XC}} \left\| (G^{(m)})^\top \lambda \right\|_2^2 + \lambda^\top (h^{(m)} - G^{(m)} Q^q) \right\}.$$

We solve this dual by projected gradient ascent on  $\lambda$ . The primal variables are then recovered as

$$C^{q+1} = Q^q + \frac{1}{\rho_{XC}} (G^{(m)})^\top \lambda^*, \quad s^{q+1} = \max\{0, h^{(m)} - G^{(m)} C^{q+1}\}.$$

- **Dual updates.** Finally, the scaled dual variables are updated by accumulating the primal residuals of the three splitting constraints:

$$\begin{aligned} U_{XV}^{q+1} &= U_{XV}^q + X^{q+1} - V^{q+1}, & U_{XC}^{q+1} &= U_{XC}^q + X^{q+1} - C^{q+1}, \\ U_Z^{q+1} &= U_Z^q + D_b V^{q+1} - Z^{q+1}. \end{aligned}$$

The  $X$ - and  $V$ -updates require solving linear systems with matrices of the form  $\alpha I + \beta D^\top D$  or  $\alpha I + \beta A^\top A$ , which are tridiagonal along the time dimension. Their factorizations can therefore be cached and reused across ADMM iterations within each SCP iteration. We implement the projector in JAX [11], using just-in-time compilation and GPU parallelism for batched inference.

For simplicity in implementation, we use fixed iteration budgets for all nested loops:  $K_{\text{cvx}}$  successive-convexification iterations,  $K_{\text{ADMM}}$  ADMM iterations, and  $K_{\text{QP}}$  projected-gradient steps for the local collision QP. Developing principled termination criteria for these loops is an interesting direction for future work and could further reduce inference-time computational overhead. We summarize the full procedure in Algorithm 2 and default parameters in Table 4.

#### D.4 Safe and diverse contact-rich manipulation

**Training.** We employ a diffusion model with noise-prediction parametrization on the augmented expert demonstrations dataset using default parameters in [20].

**Evaluation.** We follow the same setup as in [43] and generate 100 pairs of trajectories for each of 50 random starting configurations. We constrain each agent by imposing *test-time* velocity limits corresponding to the 90% quantile in the original work. Sampling is performed with a planning horizon of  $H_p = 16$ , execution horizon  $H_a = 8$ , and for a maximum of 360 environment steps.

**Cost functions.** For clarity of exposition, we repeat the definition of the cost functions used to encourage non-intersecting trajectories during coupled sampling.

*Determinantal Point Process (DPP)* [20]. Given a generated pair  $(X, Y) \in \mathbb{R}^{H \times 2 \times 2}$ , the DPP cost directly penalizes high cosine similarity between the flattened trajectories  $(\bar{X}, \bar{Y}) \in \mathbb{R}^{2H \times 2}$ :

$$c_{\text{DPP}}(X, Y) = \log(\cos \angle(\bar{X}, \bar{Y}) + \varepsilon) \quad (46)$$

where  $\varepsilon > 1$  regulates cost sharpness.

*Log-Barrier (LB)*. Given a trajectory tuple  $(X, Y) \in \mathbb{R}^{H \times 2 \times 2}$ , log-barrier cost discourages proximity of trajectories, as measured by the Euclidean distance:

$$c_{\text{LB}}(X, Y) = - \sum_{i=1}^H \log(\|X_i - Y_i\| + \alpha) \quad (47)$$

where  $\alpha > 0$  is an offset parameter.

**Projected Gradient Descent.** For the PCD-DPP and PCD-LB baselines, we use one gradient iteration per denoising step with guidance strengths of  $\gamma_{\text{DPP}} = 0.2$  and  $\gamma_{\text{LB}} = 0.02$  respectively. For DiRecT-DPP and DiRecT-LB we introduce diversity costs directly in the optimization problem (33) scaled by an appropriate weight  $\lambda_c > 0$ . For a comparison under similar computational budgets, the optimization problem is not solved to convergence, instead we employ one iteration of projected gradient descent [37]. Given a pair of denoised estimates  $(\bar{X}, \bar{Y})$ , the optimized pair  $(X^*, Y^*)$  becomes<sup>8</sup>:

$$\begin{aligned} X^* &= \Pi_{\mathcal{K}} \left( \bar{X} - \lambda_c \nabla_X c_{\text{DPP/LB}}(X, Y) \Big|_{\bar{X}, \bar{Y}} \right), \\ Y^* &= \Pi_{\mathcal{K}} \left( \bar{Y} - \lambda_c \nabla_Y c_{\text{DPP/LB}}(X, Y) \Big|_{\bar{X}, \bar{Y}} \right). \end{aligned} \quad (48)$$

Here,  $\Pi_{\mathcal{K}}$  is the same ADMM-based projector as the PCD baselines over the set  $\mathcal{K}$  of velocity-restricted trajectories. We sweep multiple weights for  $\lambda_c$  and choose  $\lambda_c = 0.005$  for DiRecT-LB and  $\lambda_c = 0.05$  for DiRecT-DPP. Additional details are provided in Appendix E.4.

<sup>8</sup>We include the step size for the gradient update in  $\lambda_c$ , instead of defining an additional hyperparameter. Moreover, the gradient of the quadratic regularization from Tweedie’s estimate vanishes at  $(\bar{X}, \bar{Y})$ .

---

**Algorithm 2:** Batched SCP–ADMM Projection for MRMP
 

---

**Input:** Tweedie reference  $\hat{X}$ , starts  $b$ , obstacle primitives  $\mathcal{O}$ , robot radius  $\delta$ , step bound  $d_{\max} = v_{\max}\Delta t$ ; iterations  $K_{\text{cvx}}, K_{\text{ADMM}}, K_{\text{QP}}$ ; penalties  $\rho_{XV}, \rho_{XC}, \rho_Z$ ; schedules  $\mu_m, \tau_m$ ; dual step size  $\alpha$

**Output:** Projected trajectory  $X$

- 1 Pre-compute  $D, A$ , and  $B$  such that  $D_b V = AV - B$ , with  $B_i^1 = b_i$  and  $B_i^k = 0$  for  $k \geq 2$ ;
- 2  $X \leftarrow \hat{X}, V \leftarrow X, C \leftarrow X$ ; // Initialize from diffusion estimate
- 3  $Z \leftarrow \Pi_{\mathcal{K}_Z}(AV - B), U_{XV}, U_{XC}, U_Z \leftarrow 0$ ; // Initialize velocity split and duals
- 4 **SCP convexification;**
- 5 **for**  $m = 0, \dots, K_{\text{cvx}} - 1$  **do**
- 6    $X_{\text{lin}} \leftarrow X$ ;
- 7   Select active constraints  $\mathcal{A}_{\text{RR}}^{(m)}, \mathcal{A}_{\text{O}}^{(m)}$  at  $X_{\text{lin}}$ ;
- 8   Build the linearized collision constraints  $G^{(m)}C + s \geq h^{(m)}, s \geq 0$ ;
- 9    $H_X \leftarrow (1 + \tau_m + \rho_{XV} + \rho_{XC})I + \lambda_{\text{sm}}D^T D$ ; // X-update system
- 10    $H_V \leftarrow \rho_{XV}I + \rho_Z A^T A$ ; // V-update system
- 11   Cache factorizations of  $H_X$  and  $H_V$ ; // Tridiagonal along time
- 12    $C \leftarrow X, s \leftarrow 0, U_{XC} \leftarrow 0$ ;
- 13   **ADMM splitting;**
- 14   **for**  $q = 0, \dots, K_{\text{ADMM}} - 1$  **do**
- 15      $X, V, Z$  **updates;**
- 16      $R_X \leftarrow \hat{X} + \tau_m X_{\text{lin}} + \rho_{XV}(V - U_{XV}) + \rho_{XC}(C - U_{XC})$ ;
- 17      $X \leftarrow \text{SOLVEBATCH}(H_X X = R_X)$ ; // Batched linear solve on GPU
- 18      $R_V \leftarrow \rho_{XV}(X + U_{XV}) + \rho_Z A^T(Z - U_Z + B)$ ;
- 19      $V \leftarrow \text{SOLVEBATCH}(H_V V = R_V)$ ; // Batched linear solve on GPU
- 20      $W \leftarrow AV - B + U_Z$ ;
- 21      $Z_i^k \leftarrow \min \left\{ 1, \frac{d_{\max}}{\|W_i^k\|_2 + \varepsilon_{\text{min}}} \right\} W_i^k, \quad i \in [N_a], k \in [H]$ ; // Project onto velocity balls
- 22     **Local collision-QP dual;**
- 23      $Q \leftarrow X + U_{XC}, \quad \lambda \leftarrow 0$ ;
- 24     **for**  $r = 0, \dots, K_{\text{QP}} - 1$  **do**
- 25        $g_\lambda \leftarrow -\rho_{XC}^{-1} G^{(m)}(G^{(m)})^T \lambda + (h^{(m)} - G^{(m)}Q)$ ; // Dual gradient
- 26        $\lambda \leftarrow \text{clip}(\lambda + \alpha g_\lambda, 0, \mu_m)$ ; // Box-constrained dual step
- 27      **$C, s$  recovery and dual updates;**
- 28      $C \leftarrow Q + \rho_{XC}^{-1}(G^{(m)})^T \lambda$ ;
- 29      $s \leftarrow \max\{0, h^{(m)} - G^{(m)}C\}$ ;
- 30      $U_{XV} \leftarrow U_{XV} + X - V$ ; // Position-velocity residual
- 31      $U_{XC} \leftarrow U_{XC} + X - C$ ; // Position-collision residual
- 32      $U_Z \leftarrow U_Z + AV - B - Z$ ; // Velocity-projection residual
- 33 **return**  $X$

---

Table 4: Main hyperparameters used by the batched SCP–ADMM MRMP optimizer.

Symbol	$K_{\text{cvx}}$	$K_{\text{ADMM}}$	$K_{\text{QP}}$	$\rho_{XV}$	$\rho_{XC}$	$\rho_Z$	$\mu_{\text{init}}$	$\mu_{\text{max}}$	$\gamma_\mu$	$\tau_{\text{init}}$	$\tau_{\text{max}}$	$\gamma_\tau$
Value	5	50	100	1.0	1.0	1.0	1.0	1000.0	2.0	0.1	10.0	1.5

## E Additional results

### E.1 Safe maze navigation

We report in Table 5 a detailed comparison of our method against additional baselines, with a focus on the difference between *generated* and *rollout* safety. We consider these additional methods for comparison: **Classifier Guidance** [17] which employs gradient guidance through *soft* violation costs without posterior sampling, **Primal-Dual** [71] as an additional Lagrangian-based method, and the two additional SafeDiffuser variations **SafeDiffuser-ReS**, and **SafeDiffuser-TVS** [69]

Table 5: Results on the Maze2D constrained navigation task. Mean values are computed over 100 i.i.d. samples and reported alongside their standard deviation. Gray columns report metrics evaluated on the planned trajectories before execution. Best value(s) in boldface.

Env	Method	SR $\uparrow$	Viol. $\downarrow$	Score $\uparrow$	Time (s) $\downarrow$	Gen. SR $\uparrow$	Gen. Viol. $\downarrow$	Gen. AS $\downarrow$	Gen. CS $\downarrow$
Maze2D Broad	Diffuser [29]	0.000	45.920 $\pm$ 11.863	<b>1.601<math>\pm</math>0.025</b>	0.316 $\pm$ 0.078	0.000 $\pm$ 0.000	49.040 $\pm$ 17.426	0.057 $\pm$ 0.005	0.636 $\pm$ 0.077
	Classifier Guidance [17]	0.030	37.480 $\pm$ 13.260	1.587 $\pm$ 0.164	0.654 $\pm$ 0.093	0.040 $\pm$ 0.197	35.760 $\pm$ 19.482	0.055 $\pm$ 0.005	0.619 $\pm$ 0.077
	Gradient Guidance [15]	0.040	25.520 $\pm$ 10.178	1.587 $\pm$ 0.164	3.637 $\pm$ 0.076	0.040 $\pm$ 0.197	10.220 $\pm$ 7.882	0.056 $\pm$ 0.005	0.636 $\pm$ 0.073
	Projected Diffusion [14]	0.220	42.000 $\pm$ 47.282	1.119 $\pm$ 0.708	46.398 $\pm$ 11.096	1.000 $\pm$ 0.000	0.000 $\pm$ 0.000	<b>0.002<math>\pm</math>0.000</b>	0.011 $\pm$ 0.004
	Primal-Dual [71]	0.170	26.610 $\pm$ 31.734	0.267 $\pm$ 0.417	5.957 $\pm$ 0.083	1.000 $\pm$ 0.000	0.000 $\pm$ 0.000	21.299 $\pm$ 0.219	1.861 $\pm$ 0.015
	Augmented Lagrangian [71]	0.080	72.920 $\pm$ 92.751	-0.010 $\pm$ 0.145	5.676 $\pm$ 0.566	0.000 $\pm$ 0.000	91.010 $\pm$ 55.079	2.152 $\pm$ 0.974	1.407 $\pm$ 0.452
	SafeDiffuser-RoS [69]	0.040	66.260 $\pm$ 41.720	1.186 $\pm$ 0.533	148.967 $\pm$ 3.831	1.000 $\pm$ 0.000	0.000 $\pm$ 0.000	0.008 $\pm$ 0.007	0.010 $\pm$ 0.004
	SafeDiffuser-ReS [69]	0.520	9.690 $\pm$ 11.948	0.907 $\pm$ 0.815	486.568 $\pm$ 61.073	1.000 $\pm$ 0.000	0.000 $\pm$ 0.000	0.003 $\pm$ 0.003	0.015 $\pm$ 0.006
	SafeDiffuser-TVS [69]	0.040	62.240 $\pm$ 38.460	1.219 $\pm$ 0.561	128.758 $\pm$ 2.988	1.000 $\pm$ 0.000	0.000 $\pm$ 0.000	0.005 $\pm$ 0.004	0.010 $\pm$ 0.004
	<b>DiRecT (Ours)</b>	<b>0.970</b>	<b>0.450<math>\pm</math>3.806</b>	1.500 $\pm$ 0.419	17.657 $\pm$ 0.629	1.000 $\pm$ 0.000	0.000 $\pm$ 0.000	<b>0.002<math>\pm</math>0.000</b>	<b>0.008<math>\pm</math>0.002</b>
Maze2D Narrow	Diffuser [29]	0.000	103.940 $\pm$ 21.881	1.601 $\pm$ 0.025	0.321 $\pm$ 0.086	0.000 $\pm$ 0.000	101.230 $\pm$ 24.551	0.057 $\pm$ 0.005	0.636 $\pm$ 0.077
	Classifier Guidance [17]	0.000	85.280 $\pm$ 24.224	1.608 $\pm$ 0.022	0.695 $\pm$ 0.079	0.000 $\pm$ 0.000	76.120 $\pm$ 26.527	0.056 $\pm$ 0.005	0.629 $\pm$ 0.077
	Gradient Guidance [15]	0.000	51.300 $\pm$ 19.221	1.619 $\pm$ 0.029	3.608 $\pm$ 0.023	0.000 $\pm$ 0.000	23.390 $\pm$ 14.123	0.056 $\pm$ 0.005	0.647 $\pm$ 0.072
	Projected Diffusion [14]	0.780	37.290 $\pm$ 129.876	0.163 $\pm$ 0.459	112.918 $\pm$ 19.517	0.420 $\pm$ 0.496	17.630 $\pm$ 30.680	0.018 $\pm$ 0.039	0.033 $\pm$ 0.077
	Primal-Dual [71]	0.000	55.970 $\pm$ 49.478	0.268 $\pm$ 0.418	5.154 $\pm$ 0.464	0.910 $\pm$ 0.288	0.110 $\pm$ 0.373	21.306 $\pm$ 0.226	1.861 $\pm$ 0.014
	Augmented Lagrangian [71]	0.000	217.510 $\pm$ 159.431	0.156 $\pm$ 0.449	6.022 $\pm$ 0.122	0.000 $\pm$ 0.000	197.520 $\pm$ 45.739	5.516 $\pm$ 1.301	1.765 $\pm$ 0.040
	SafeDiffuser-RoS [69]	0.000	278.870 $\pm$ 209.870	0.735 $\pm$ 0.681	509.850 $\pm$ 19.929	0.000 $\pm$ 0.000	136.250 $\pm$ 39.029	0.419 $\pm$ 0.168	0.350 $\pm$ 0.148
	SafeDiffuser-ReS [69]	0.370	79.090 $\pm$ 161.395	1.155 $\pm$ 0.764	1423.534 $\pm$ 41.319	0.760 $\pm$ 0.429	6.320 $\pm$ 16.578	0.031 $\pm$ 0.084	0.078 $\pm$ 0.164
	SafeDiffuser-TVS [69]	0.000	315.040 $\pm$ 223.000	0.729 $\pm$ 0.694	384.860 $\pm$ 9.681	0.000 $\pm$ 0.000	35.460 $\pm$ 12.962	0.059 $\pm$ 0.026	0.038 $\pm$ 0.011
	<b>DiRecT (Ours)</b>	<b>0.940</b>	<b>0.230<math>\pm</math>1.038</b>	<b>1.624<math>\pm</math>0.027</b>	98.093 $\pm$ 5.047	1.000 $\pm$ 0.000	0.000 $\pm$ 0.000	<b>0.002<math>\pm</math>0.000</b>	<b>0.010<math>\pm</math>0.006</b>

for CBF-based constraining. We also report additional metrics on the *generated* trajectory: (i) *Safety Rate*, measuring the fraction of samples that correctly avoid obstacles; (ii) mean *Violations*, measuring the number of steps the predicted trajectory remains infeasible; (iii) *Acceleration Smoothness* (AS), quantifying the change in velocity across the trajectory, and computed as the magnitude of the second-order position differences averaged across all planned transitions:  $AS = (H - 2)^{-1} \sum_{i=1}^{H-2} \|s_{i+1} - 2s_i + s_{i-1}\|$ ; (iv) *Curvature Smoothness* (CS), measuring the mean curvature of the generated trajectory. Following [16], we define the turning angle  $\theta_i = \cos^{-1}(w_i^T w_{i+1} / (\|w_i\| \|w_{i+1}\|))$ ,  $w_i = s_{i+1} - s_i$ ,  $i = 0, \dots, H - 3$ , and compute the metric as the average across the planned horizon  $CS = (H - 2)^{-1} \sum_{i=0}^{H-3} (1 - \cos \theta_i)$ .

In both variants DiRecT outperforms all other baselines in terms of *rollout* safety. Even though Projected Diffusion, Primal-Dual and the three SafeDiffuser variations generate safe trajectories at planning time on the broad instance of the problem, their rollout performance remains limited. This can be explained by noting that these methods find feasible solutions to the optimization problem by departing substantially from the data distribution. As shown in Figures 7–8, prior methods in highly constrained dynamic settings often produce trajectories that depart from the learned maze structure and pass through maze walls. In contrast, our method performs optimization near the data manifold, thereby remaining proximal to the data distribution. In the narrow setting, we observe that IPOPT struggles to find feasible solutions within the allowed 200 iterations, sometimes leading to infeasible generated solutions for projection-based methods. Moreover, primal-dual methods and some SafeDiffuser variants exhibit instabilities on certain samples under dynamic constraints.

## E.2 Safe robotic manipulation

We compare the same extended baselines as in Table 5 and report safety and success rates of these additional policies in Table 6. Our method is the only one to obtain perfect task success rate.

For the primal-dual implementation, we tuned the reference hyperparameters to the best of our ability, including the dual-ascent learning rate. Nevertheless, in the highly constrained setting with dynamics constraints, the method exhibited increasing instability, occasionally producing trajectories that triggered errors in the MuJoCo simulator during execution.

Table 6: Results on the D3IL avoiding constrained manipulation task. Mean values are computed over 100 i.i.d. trials and reported with standard deviations where applicable. Best value in boldface.

Method	SR $\uparrow$	Task $\uparrow$	Steps (Safe) $\downarrow$	Time (s) $\downarrow$
Diffuser [29]	0.060	0.960	70.30 $\pm$ 11.83	0.224 $\pm$ 0.002
Classifier Guidance [17]	0.000	0.000	–	0.627 $\pm$ 0.030
Gradient Guidance [15]	0.880	0.980	62.58 $\pm$ 7.05	6.615 $\pm$ 0.540
Projected Diffusion [14]	0.770	0.970	63.77 $\pm$ 6.88	1.367 $\pm$ 0.057
Primal-Dual [71]	–	–	–	–
Augmented Lagrangian [71]	0.220	0.840	63.45 $\pm$ 7.22	4.152 $\pm$ 0.018
SafeDiffuser-RoS [69]	0.370	0.820	63.19 $\pm$ 11.56	18.890 $\pm$ 0.877
SafeDiffuser-ReS [69]	0.220	0.860	62.09 $\pm$ 9.62	12.949 $\pm$ 0.839
SafeDiffuser-TVS [69]	0.300	0.850	<b>60.57<math>\pm</math>8.49</b>	13.278 $\pm$ 0.488
<b>DiRecT (Ours)</b>	<b>1.000</b>	<b>1.000</b>	62.86 $\pm$ 6.90	0.688 $\pm$ 0.061

### E.3 Safe multi-robot motion planning

We present sweep results for each of the three velocity limitations and number of agents in Tables 7, 8, 9, 10. We report computational times as well as the mean number of collisions. DiRecT consistently improves *Success* and *Constraint safety*. On *Empty* and *Highways*, our method matches the *data adherence* of the pretrained model for all velocity limitations. We note that on *Conveyor* and *Drop-Region* comparing data adherence between DiRecT and the PCD variants is not straightforward for  $N \in \{12, 16, 20\}$ , as the latter are not capable of generating feasible trajectories, thereby showcasing high task success while neglecting safety.

Table 7: MRMP results on *Empty*. SR: success rate (%), CS: constraint safety (%), Coll: mean collisions, DA: data adherence, Time: computation time (s). Standard deviations are over different initializations and boldface represents best among the methods actively enforcing constraints.

# Ag.	Method	Low ( $v_{\max}=0.675$ )					Medium ( $v_{\max}=0.692$ )					High ( $v_{\max}=0.703$ )				
		SR $\uparrow$	CS $\uparrow$	Coll $\downarrow$	DA $\uparrow$	Time (s) $\downarrow$	SR $\uparrow$	CS $\uparrow$	Coll $\downarrow$	DA $\uparrow$	Time (s) $\downarrow$	SR $\uparrow$	CS $\uparrow$	Coll $\downarrow$	DA $\uparrow$	Time (s) $\downarrow$
4	Diffuser	65.0	61.7 $\pm$ 47.4	1.15 $\pm$ 1.74	0.997 $\pm$ 0.018	1.0 $\pm$ 0.4	65.0	61.7 $\pm$ 47.4	1.15 $\pm$ 1.74	0.997 $\pm$ 0.018	1.0 $\pm$ 0.4	65.0	61.7 $\pm$ 47.4	1.15 $\pm$ 1.74	0.997 $\pm$ 0.018	1.0 $\pm$ 0.4
	MMD-CBS	100.0	100.0	0.00	–	5.5 $\pm$ 0.7	100.0	100.0	0.00	–	5.5 $\pm$ 0.7	100.0	100.0	0.00	–	5.5 $\pm$ 0.7
	PCD-LB	85.0	81.4 $\pm$ 34.5	0.41 $\pm$ 0.90	0.739 $\pm$ 0.102	3.0 $\pm$ 1.5	75.0	73.3 $\pm$ 44.0	0.60 $\pm$ 1.08	0.984 $\pm$ 0.052	2.0	87.0	82.6 $\pm$ 33.5	0.39 $\pm$ 0.85	0.736 $\pm$ 0.102	2.8 $\pm$ 1.3
	PCD-SHD	90.0	86.4 $\pm$ 31.8	0.27 $\pm$ 0.68	0.994 $\pm$ 0.020	2.0 $\pm$ 0.3	93.0	87.2 $\pm$ 30.8	0.22 $\pm$ 0.53	0.994 $\pm$ 0.020	1.9	95.0	90.0 $\pm$ 25.1	0.16 $\pm$ 0.42	0.994 $\pm$ 0.020	2.0 $\pm$ 0.1
	Final Proj.	89.0	84.7 $\pm$ 35.1	0.26 $\pm$ 0.80	0.997 $\pm$ 0.017	2.9 $\pm$ 0.4	97.0	94.8 $\pm$ 20.1	0.14 $\pm$ 0.68	<b>0.998<math>\pm</math>0.015</b>	2.3	97.0	96.1 $\pm$ 18.1	0.11 $\pm$ 0.57	<b>0.998<math>\pm</math>0.017</b>	3.7 $\pm$ 2.3
	DiRecT (Ours)	<b>98.0</b>	<b>98.0<math>\pm</math>14.0</b>	<b>0.05<math>\pm</math>0.35</b>	<b>0.998<math>\pm</math>0.016</b>	31.1 $\pm$ 0.9	<b>98.0</b>	<b>98.0<math>\pm</math>14.0</b>	<b>0.05<math>\pm</math>0.34</b>	<b>0.998<math>\pm</math>0.015</b>	19.8	<b>99.0</b>	<b>98.2<math>\pm</math>12.6</b>	<b>0.04<math>\pm</math>0.31</b>	<b>0.998<math>\pm</math>0.016</b>	29.4 $\pm$ 11.9
8	Diffuser	15.0	9.4 $\pm$ 28.2	6.20 $\pm$ 4.44	0.996 $\pm$ 0.015	0.9 $\pm$ 0.4	15.0	9.4 $\pm$ 28.2	6.20 $\pm$ 4.44	0.996 $\pm$ 0.015	0.9 $\pm$ 0.4	15.0	9.4 $\pm$ 28.2	6.20 $\pm$ 4.44	0.996 $\pm$ 0.015	0.9 $\pm$ 0.4
	MMD-CBS	100.0	100.0	0.00	–	13.3 $\pm$ 0.2	100.0	100.0	0.00	–	13.3 $\pm$ 0.2	100.0	100.0	0.00	–	13.3 $\pm$ 0.2
	PCD-LB	40.5	22.1 $\pm$ 36.7	3.35 $\pm$ 2.85	0.744 $\pm$ 0.073	6.0 $\pm$ 2.0	25.0	19.7 $\pm$ 38.1	3.91 $\pm$ 3.55	0.977 $\pm$ 0.041	4.1	40.5	23.4 $\pm$ 37.8	3.06 $\pm$ 2.58	0.743 $\pm$ 0.074	5.3 $\pm$ 2.0
	PCD-SHD	74.0	58.9 $\pm$ 44.2	1.15 $\pm$ 1.64	0.985 $\pm$ 0.022	3.9 $\pm$ 0.2	77.0	66.3 $\pm$ 41.8	0.89 $\pm$ 1.36	0.986 $\pm$ 0.022	3.6	82.0	68.8 $\pm$ 40.7	0.74 $\pm$ 1.12	0.986 $\pm$ 0.022	2.8 $\pm$ 0.2
	Final Proj.	45.0	31.6 $\pm$ 43.2	2.11 $\pm$ 2.57	<b>0.995<math>\pm</math>0.016</b>	2.7 $\pm$ 0.3	73.0	57.7 $\pm$ 45.0	1.22 $\pm$ 2.06	0.995 $\pm$ 0.015	2.1	79.0	66.1 $\pm$ 43.3	0.93 $\pm$ 1.69	<b>0.995<math>\pm</math>0.015</b>	3.3 $\pm$ 1.6
	DiRecT (Ours)	<b>95.0</b>	<b>94.0<math>\pm</math>22.8</b>	<b>0.13<math>\pm</math>0.55</b>	<b>0.995<math>\pm</math>0.015</b>	26.5 $\pm$ 7.4	<b>96.0</b>	<b>93.1<math>\pm</math>24.1</b>	<b>0.13<math>\pm</math>0.52</b>	<b>0.996<math>\pm</math>0.015</b>	23.9	<b>97.0</b>	<b>94.3<math>\pm</math>22.2</b>	<b>0.12<math>\pm</math>0.53</b>	<b>0.995<math>\pm</math>0.015</b>	29.8 $\pm$ 12.1
12	Diffuser	1.0	1.0 $\pm$ 9.9	14.52 $\pm$ 7.73	0.998 $\pm$ 0.006	1.0 $\pm$ 0.2	1.0	1.0 $\pm$ 9.9	14.52 $\pm$ 7.73	0.998 $\pm$ 0.006	1.0 $\pm$ 0.2	1.0	1.0 $\pm$ 9.9	14.52 $\pm$ 7.73	0.998 $\pm$ 0.006	1.0 $\pm$ 0.2
	MMD-CBS	100.0	100.0	0.00	–	56.9 $\pm$ 2.4	100.0	100.0	0.00	–	56.9 $\pm$ 2.4	100.0	100.0	0.00	–	56.9 $\pm$ 2.4
	PCD-LB	3.0	1.3 $\pm$ 9.3	11.43 $\pm$ 5.65	0.748 $\pm$ 0.050	6.2 $\pm$ 2.6	2.0	2.0 $\pm$ 14.0	11.04 $\pm$ 6.40	0.987 $\pm$ 0.022	3.7	2.5	1.3 $\pm$ 9.4	10.78 $\pm$ 5.36	0.748 $\pm$ 0.050	5.1 $\pm$ 1.9
	PCD-SHD	34.0	18.8 $\pm$ 31.9	2.97 $\pm$ 2.66	0.984 $\pm$ 0.013	3.8 $\pm$ 0.7	48.0	27.8 $\pm$ 35.7	2.25 $\pm$ 2.10	0.984 $\pm$ 0.013	3.9	62.0	32.6 $\pm$ 37.6	1.90 $\pm$ 1.79	0.984 $\pm$ 0.013	3.5 $\pm$ 0.2
	Final Proj.	25.0	15.7 $\pm$ 33.8	4.80 $\pm$ 4.40	<b>0.997<math>\pm</math>0.006</b>	4.4 $\pm$ 1.0	51.0	32.9 $\pm$ 44.0	2.98 $\pm$ 3.65	<b>0.997<math>\pm</math>0.006</b>	3.6	62.0	48.9 $\pm$ 46.0	2.18 $\pm$ 3.09	<b>0.997<math>\pm</math>0.006</b>	4.4 $\pm$ 0.9
	DiRecT (Ours)	<b>95.5</b>	<b>90.5<math>\pm</math>27.7</b>	<b>0.24<math>\pm</math>0.78</b>	<b>0.997<math>\pm</math>0.007</b>	42.6 $\pm$ 2.8	<b>95.0</b>	<b>87.0<math>\pm</math>30.4</b>	<b>0.30<math>\pm</math>0.83</b>	<b>0.997<math>\pm</math>0.007</b>	37.0	<b>95.5</b>	<b>87.3<math>\pm</math>29.7</b>	<b>0.29<math>\pm</math>0.76</b>	<b>0.997<math>\pm</math>0.007</b>	39.5 $\pm$ 1.4
16	Diffuser	0.0	0.0 $\pm$ 0.0	26.17 $\pm$ 9.98	0.998 $\pm$ 0.006	1.4 $\pm$ 0.4	0.0	0.0 $\pm$ 0.0	26.17 $\pm$ 9.98	0.998 $\pm$ 0.006	1.4 $\pm$ 0.4	0.0	0.0 $\pm$ 0.0	26.17 $\pm$ 9.98	0.998 $\pm$ 0.006	1.4 $\pm$ 0.4
	MMD-CBS	100.0	100.0	0.00	–	48.0 $\pm$ 3.3	100.0	100.0	0.00	–	48.0 $\pm$ 3.3	100.0	100.0	0.00	–	48.0 $\pm$ 3.3
	PCD-LB	0.0	0.0 $\pm$ 0.0	30.57 $\pm$ 9.83	0.740 $\pm$ 0.044	8.7 $\pm$ 3.8	0.0	0.0 $\pm$ 0.0	21.22 $\pm$ 8.61	0.986 $\pm$ 0.023	5.4	0.0	0.0 $\pm$ 0.0	29.78 $\pm$ 9.75	0.740 $\pm$ 0.044	6.7 $\pm$ 2.0
	PCD-SHD	19.0	7.0 $\pm$ 19.0	6.18 $\pm$ 3.71	0.979 $\pm$ 0.018	6.7 $\pm$ 0.9	29.0	10.4 $\pm$ 23.9	4.85 $\pm$ 3.13	0.979 $\pm$ 0.017	5.2	29.0	12.4 $\pm$ 25.1	4.12 $\pm$ 2.76	0.979 $\pm$ 0.017	4.9 $\pm$ 0.3
	Final Proj.	5.0	2.6 $\pm$ 11.9	9.16 $\pm$ 5.09	<b>0.995<math>\pm</math>0.007</b>	6.4 $\pm$ 1.1	22.0	12.1 $\pm$ 28.6	5.66 $\pm$ 4.07	0.995 $\pm$ 0.007	5.7	36.5	20.1 $\pm$ 35.2	4.23 $\pm$ 3.51	0.995 $\pm$ 0.007	5.7 $\pm$ 0.3
	DiRecT (Ours)	<b>90.0</b>	<b>80.4<math>\pm</math>35.4</b>	<b>0.57<math>\pm</math>1.30</b>	<b>0.995<math>\pm</math>0.007</b>	58.2 $\pm$ 3.7	<b>93.0</b>	<b>78.7<math>\pm</math>37.4</b>	<b>0.54<math>\pm</math>1.16</b>	<b>0.996<math>\pm</math>0.007</b>	59.1	<b>93.0</b>	<b>81.8<math>\pm</math>34.5</b>	<b>0.42<math>\pm</math>0.95</b>	<b>0.996<math>\pm</math>0.007</b>	60.9 $\pm$ 0.9
20	Diffuser	0.0	0.0 $\pm$ 0.0	40.39 $\pm$ 14.13	0.998 $\pm$ 0.006	1.7 $\pm$ 0.4	0.0	0.0 $\pm$ 0.0	40.39 $\pm$ 14.13	0.998 $\pm$ 0.006	1.7 $\pm$ 0.4	0.0	0.0 $\pm$ 0.0	40.39 $\pm$ 14.13	0.998 $\pm$ 0.006	1.7 $\pm$ 0.4
	MMD-CBS	33.3	46.7	14.67	–	69.2 $\pm$ 8.5	33.3	46.7	14.67	–	69.2 $\pm$ 8.5	33.3	46.7	14.67	–	69.2 $\pm$ 8.5
	PCD-LB	0.0	0.0 $\pm$ 0.0	34.43 $\pm$ 12.76	0.988 $\pm$ 0.018	8.7	0.0	0.0 $\pm$ 0.0	33.09 $\pm$ 12.23	0.988 $\pm$ 0.018	8.0	0.0	0.0 $\pm$ 0.0	32.03 $\pm$ 11.73	0.988 $\pm$ 0.018	7.6
	PCD-SHD	7.0	2.7 $\pm$ 12.5	9.07 $\pm$ 4.94	0.973 $\pm$ 0.018	7.1	11.0	4.1 $\pm$ 16.3	7.20 $\pm$ 4.10	0.973 $\pm$ 0.018	8.1	19.0	5.5 $\pm$ 18.4	6.07 $\pm$ 3.45	0.973 $\pm$ 0.018	8.0
	Final Proj.	1.0	0.0 $\pm$ 0.4	13.54 $\pm$ 7.95	0.995 $\pm$ 0.007	9.3 $\pm$ 2.8	13.0	4.7 $\pm$ 16.5	8.24 $\pm$ 6.38	0.995 $\pm$ 0.007	8.1	23.0	11.3 $\pm$ 25.5	6.37 $\pm$ 5.59	0.995 $\pm$ 0.007	8.1 $\pm$ 0.2
	DiRecT (Ours)	<b>90.0</b>	<b>76.1<math>\pm</math>39.0</b>	<b>0.82<math>\pm</math>1.88</b>	<b>0.996<math>\pm</math>0.007</b>	80.7	<b>87.0</b>	<b>77.5<math>\pm</math>37.5</b>	<b>0.76<math>\pm</math>1.71</b>	<b>0.996<math>\pm</math>0.007</b>	87.2	<b>90.0</b>	<b>80.9<math>\pm</math>35.3</b>	<b>0.62<math>\pm</math>1.48</b>	<b>0.996<math>\pm</math>0.007</b>	89.6

Table 8: MRMP results on Highways. SR: success rate (%), CS: constraint safety (%), Coll: mean collisions, DA: data adherence, Time: computation time (s). Standard deviations are over different initializations and boldface represents best among the methods actively enforcing constraints.

# Ag.	Method	Low ( $v_{max}=0.647$ )					Medium ( $v_{max}=0.781$ )					High ( $v_{max}=0.878$ )				
		SR $\uparrow$	CS $\uparrow$	Coll $\downarrow$	DA $\uparrow$	Time (s) $\downarrow$	SR $\uparrow$	CS $\uparrow$	Coll $\downarrow$	DA $\uparrow$	Time (s) $\downarrow$	SR $\uparrow$	CS $\uparrow$	Coll $\downarrow$	DA $\uparrow$	Time (s) $\downarrow$
4	Diffuser	54.0	16.2 $\pm$ 30.5	8.91 $\pm$ 7.89	0.994 $\pm$ 0.034	0.5 $\pm$ 0.2	54.0	16.2 $\pm$ 30.5	8.91 $\pm$ 7.89	0.994 $\pm$ 0.034	0.5 $\pm$ 0.2	54.0	16.2 $\pm$ 30.5	8.91 $\pm$ 7.89	0.994 $\pm$ 0.034	0.5 $\pm$ 0.2
	MMD-CBS	100.0	100.0	0.00	-	5.2 $\pm$ 0.6	100.0	100.0	0.00	-	5.2 $\pm$ 0.6	100.0	100.0	0.00	-	5.2 $\pm$ 0.6
	PCD-LB	94.0	60.4 $\pm$ 38.8	0.82 $\pm$ 1.20	0.977 $\pm$ 0.066	1.9	98.0	69.6 $\pm$ 32.3	0.82 $\pm$ 1.12	0.980 $\pm$ 0.062	1.9	48.5	34.2 $\pm$ 15.8	0.44 $\pm$ 0.59	0.938 $\pm$ 0.085	1.8 $\pm$ 0.1
	PCD-SHD	96.0	78.1 $\pm$ 31.9	0.07 $\pm$ 0.20	0.978 $\pm$ 0.064	1.8	100.0	93.6 $\pm$ 9.6	0.03 $\pm$ 0.04	0.980 $\pm$ 0.060	2.0	100.0	94.9 $\pm$ 8.3	0.02 $\pm$ 0.05	0.981 $\pm$ 0.058	1.8 $\pm$ 0.0
	Final Proj.	99.0	76.7 $\pm$ 30.4	0.72 $\pm$ 1.52	0.994 $\pm$ 0.034	2.5	100.0	99.5 $\pm$ 3.8	0.01 $\pm$ 0.08	0.994 $\pm$ 0.034	2.5	100.0	100.0 $\pm$ 0.0	0.00 $\pm$ 0.00	0.994 $\pm$ 0.034	4.4 $\pm$ 2.5
	DiRecT (Ours)	100.0	100.0 $\pm$ 0.0	0.00 $\pm$ 0.00	0.993 $\pm$ 0.035	28.5	100.0	100.0 $\pm$ 0.0	0.00 $\pm$ 0.00	0.993 $\pm$ 0.035	28.6	100.0	100.0 $\pm$ 0.0	0.00 $\pm$ 0.00	0.993 $\pm$ 0.035	49.2 $\pm$ 27.6
8	Diffuser	2.0	0.1 $\pm$ 0.9	39.77 $\pm$ 18.43	0.992 $\pm$ 0.025	0.5 $\pm$ 0.2	2.0	0.1 $\pm$ 0.9	39.77 $\pm$ 18.43	0.992 $\pm$ 0.025	0.5 $\pm$ 0.2	2.0	0.1 $\pm$ 0.9	39.77 $\pm$ 18.43	0.992 $\pm$ 0.025	0.5 $\pm$ 0.2
	MMD-CBS	100.0	100.0	0.00	-	42.7 $\pm$ 2.0	100.0	100.0	0.00	-	42.7 $\pm$ 2.0	100.0	100.0	0.00	-	42.7 $\pm$ 2.0
	PCD-LB	63.0	11.1 $\pm$ 18.6	5.12 $\pm$ 3.42	0.972 $\pm$ 0.047	2.5	72.0	12.3 $\pm$ 20.5	6.16 $\pm$ 3.28	0.975 $\pm$ 0.043	2.5	27.0	3.3 $\pm$ 5.9	3.83 $\pm$ 2.00	0.949 $\pm$ 0.056	2.5 $\pm$ 0.4
	PCD-SHD	91.0	38.5 $\pm$ 34.3	0.37 $\pm$ 0.47	0.973 $\pm$ 0.045	2.4	100.0	64.3 $\pm$ 26.5	0.23 $\pm$ 0.29	0.976 $\pm$ 0.041	2.4	100.0	69.2 $\pm$ 23.0	0.15 $\pm$ 0.17	0.977 $\pm$ 0.040	2.3 $\pm$ 0.1
	Final Proj.	88.0	30.9 $\pm$ 32.1	4.22 $\pm$ 4.10	0.992 $\pm$ 0.025	3.5	100.0	98.1 $\pm$ 5.6	0.07 $\pm$ 0.27	0.992 $\pm$ 0.025	3.5	100.0	99.8 $\pm$ 1.1	0.01 $\pm$ 0.07	0.992 $\pm$ 0.025	4.9 $\pm$ 1.9
	DiRecT (Ours)	100.0	100.0 $\pm$ 0.0	0.00 $\pm$ 0.01	0.991 $\pm$ 0.026	40.4	100.0	100.0 $\pm$ 0.0	0.00 $\pm$ 0.00	0.992 $\pm$ 0.026	40.3	100.0	100.0 $\pm$ 0.0	0.00 $\pm$ 0.00	0.992 $\pm$ 0.026	54.3 $\pm$ 19.9
12	Diffuser	0.0	0.0 $\pm$ 0.0	91.38 $\pm$ 23.06	0.991 $\pm$ 0.022	0.6 $\pm$ 0.3	0.0	0.0 $\pm$ 0.0	91.38 $\pm$ 23.06	0.991 $\pm$ 0.022	0.6 $\pm$ 0.3	0.0	0.0 $\pm$ 0.0	91.38 $\pm$ 23.06	0.991 $\pm$ 0.022	0.6 $\pm$ 0.3
	MMD-CBS	33.3	63.9	3.67	-	59.5 $\pm$ 2.4	33.3	63.9	3.67	-	59.5 $\pm$ 2.4	33.3	63.9	3.67	-	59.5 $\pm$ 2.4
	PCD-LB	9.0	0.5 $\pm$ 3.1	19.54 $\pm$ 8.23	0.971 $\pm$ 0.044	3.6	1.0	0.0 $\pm$ 0.1	25.21 $\pm$ 8.56	0.974 $\pm$ 0.041	2.8	0.0	0.0 $\pm$ 0.0	17.40 $\pm$ 5.68	0.952 $\pm$ 0.044	2.9 $\pm$ 0.4
	PCD-SHD	78.0	11.9 $\pm$ 19.2	1.05 $\pm$ 0.90	0.972 $\pm$ 0.042	3.1	99.0	26.1 $\pm$ 21.2	0.63 $\pm$ 0.51	0.975 $\pm$ 0.039	2.9	100.0	30.3 $\pm$ 20.3	0.44 $\pm$ 0.33	0.976 $\pm$ 0.038	2.6 $\pm$ 0.1
	Final Proj.	55.0	7.5 $\pm$ 15.7	11.73 $\pm$ 6.72	0.991 $\pm$ 0.022	5.4	100.0	92.4 $\pm$ 10.7	0.31 $\pm$ 0.51	0.991 $\pm$ 0.022	5.4	100.0	99.7 $\pm$ 0.6	0.01 $\pm$ 0.02	0.991 $\pm$ 0.022	5.8 $\pm$ 0.6
	DiRecT (Ours)	100.0	99.7 $\pm$ 1.4	0.01 $\pm$ 0.03	0.990 $\pm$ 0.023	65.0	100.0	100.0 $\pm$ 0.0	0.00 $\pm$ 0.00	0.990 $\pm$ 0.023	64.7	100.0	100.0 $\pm$ 0.0	0.00 $\pm$ 0.00	0.990 $\pm$ 0.023	65.8 $\pm$ 2.0
16	Diffuser	0.0	0.0 $\pm$ 0.0	165.86 $\pm$ 31.12	0.995 $\pm$ 0.014	0.8 $\pm$ 0.3	0.0	0.0 $\pm$ 0.0	165.86 $\pm$ 31.12	0.995 $\pm$ 0.014	0.8 $\pm$ 0.3	0.0	0.0 $\pm$ 0.0	165.86 $\pm$ 31.12	0.995 $\pm$ 0.014	0.8 $\pm$ 0.3
	MMD-CBS	0.0	6.2	27.00	-	72.4 $\pm$ 4.1	0.0	6.2	27.00	-	72.4 $\pm$ 4.1	0.0	6.2	27.00	-	72.4 $\pm$ 4.1
	PCD-LB	1.0	0.1 $\pm$ 0.6	45.62 $\pm$ 12.48	0.973 $\pm$ 0.033	3.8	0.0	0.0 $\pm$ 0.0	56.59 $\pm$ 12.29	0.976 $\pm$ 0.031	3.7	0.0	0.0 $\pm$ 0.0	43.82 $\pm$ 9.83	0.956 $\pm$ 0.039	3.8 $\pm$ 0.7
	PCD-SHD	41.0	3.9 $\pm$ 10.0	2.16 $\pm$ 1.43	0.975 $\pm$ 0.031	3.8	80.0	8.6 $\pm$ 12.3	1.49 $\pm$ 1.01	0.978 $\pm$ 0.029	3.6	87.0	9.1 $\pm$ 11.5	1.06 $\pm$ 0.66	0.979 $\pm$ 0.028	3.4 $\pm$ 0.1
	Final Proj.	19.0	2.0 $\pm$ 0.2	27.99 $\pm$ 14.18	0.994 $\pm$ 0.014	7.7	100.0	74.5 $\pm$ 23.2	1.34 $\pm$ 1.96	0.994 $\pm$ 0.014	7.8	100.0	98.7 $\pm$ 4.0	0.04 $\pm$ 0.14	0.994 $\pm$ 0.014	8.2 $\pm$ 0.6
	DiRecT (Ours)	100.0	97.7 $\pm$ 7.7	0.07 $\pm$ 0.32	0.994 $\pm$ 0.015	93.6	100.0	99.9 $\pm$ 1.2	0.00 $\pm$ 0.04	0.994 $\pm$ 0.015	93.8	100.0	100.0 $\pm$ 0.0	0.00 $\pm$ 0.00	0.994 $\pm$ 0.015	94.4 $\pm$ 1.7
20	Diffuser	0.0	0.0 $\pm$ 0.0	272.99 $\pm$ 46.77	0.992 $\pm$ 0.017	0.8 $\pm$ 0.3	0.0	0.0 $\pm$ 0.0	272.99 $\pm$ 46.77	0.992 $\pm$ 0.017	0.8 $\pm$ 0.3	0.0	0.0 $\pm$ 0.0	272.99 $\pm$ 46.77	0.992 $\pm$ 0.017	0.8 $\pm$ 0.3
	MMD-CBS	0.0	0.0	35.00	-	73.8 $\pm$ 5.2	0.0	0.0	35.00	-	73.8 $\pm$ 5.2	0.0	0.0	35.00	-	73.8 $\pm$ 5.2
	PCD-LB	0.0	0.0 $\pm$ 0.0	85.17 $\pm$ 18.69	0.973 $\pm$ 0.032	5.2	0.0	0.0 $\pm$ 0.0	105.16 $\pm$ 19.39	0.976 $\pm$ 0.030	4.3	0.0	0.0 $\pm$ 0.0	120.10 $\pm$ 19.24	0.978 $\pm$ 0.028	3.8
	PCD-SHD	11.0	0.2 $\pm$ 0.7	4.07 $\pm$ 1.96	0.974 $\pm$ 0.030	4.8	39.0	1.0 $\pm$ 2.3	2.63 $\pm$ 1.22	0.977 $\pm$ 0.028	4.2	43.0	1.2 $\pm$ 2.5	1.94 $\pm$ 0.85	0.978 $\pm$ 0.027	3.8
	Final Proj.	1.0	0.0 $\pm$ 0.2	52.60 $\pm$ 22.60	0.992 $\pm$ 0.018	10.4	100.0	49.9 $\pm$ 30.6	4.15 $\pm$ 4.45	0.992 $\pm$ 0.018	10.4	100.0	96.1 $\pm$ 5.8	0.14 $\pm$ 0.25	0.992 $\pm$ 0.018	10.8 $\pm$ 0.6
	DiRecT (Ours)	100.0	95.2 $\pm$ 8.1	0.17 $\pm$ 0.37	0.992 $\pm$ 0.018	126.8	100.0	100.0 $\pm$ 0.1	0.00 $\pm$ 0.00	0.992 $\pm$ 0.018	126.8	100.0	100.0 $\pm$ 0.0	0.00 $\pm$ 0.00	0.992 $\pm$ 0.018	128.9

Table 9: MRMP results on Conveyor. SR: success rate (%), CS: constraint safety (%), Coll: mean collisions, DA: data adherence, Time: computation time (s). Standard deviations are over different initializations and boldface represents best among the methods actively enforcing constraints.

# Ag.	Method	Low ( $v_{max}=1.21$ )					Medium ( $v_{max}=1.46$ )					High ( $v_{max}=1.76$ )				
		SR $\uparrow$	CS $\uparrow$	Coll $\downarrow$	DA $\uparrow$	Time (s) $\downarrow$	SR $\uparrow$	CS $\uparrow$	Coll $\downarrow$	DA $\uparrow$	Time (s) $\downarrow$	SR $\uparrow$	CS $\uparrow$	Coll $\downarrow$	DA $\uparrow$	Time (s) $\downarrow$
4	Diffuser	1.0	0.0 $\pm$ 0.1	8.78 $\pm$ 4.23	0.960 $\pm$ 0.039	1.1 $\pm$ 0.3	1.0	0.0 $\pm$ 0.1	8.78 $\pm$ 4.23	0.960 $\pm$ 0.039	1.1 $\pm$ 0.3	1.0	0.0 $\pm$ 0.1	8.78 $\pm$ 4.23	0.960 $\pm$ 0.039	1.1 $\pm$ 0.3
	MMD-CBS	100.0	100.0	0.00	-	6.9 $\pm$ 0.8	100.0	100.0	0.00	-	6.9 $\pm$ 0.8	100.0	100.0	0.00	-	6.9 $\pm$ 0.8
	PCD-LB	100.0	24.9 $\pm$ 14.1	0.94 $\pm$ 0.42	0.896 $\pm$ 0.077	2.0	100.0	39.6 $\pm$ 15.1	0.91 $\pm$ 0.39	0.968 $\pm$ 0.032	1.9	100.0	41.8 $\pm$ 15.3	0.96 $\pm$ 0.42	0.986 $\pm$ 0.022	1.8
	PCD-SHD	100.0	28.6 $\pm$ 15.9	0.09 $\pm$ 0.08	0.902 $\pm$ 0.069	2.1	100.0	42.0 $\pm$ 17.5	0.04 $\pm$ 0.05	0.964 $\pm$ 0.030	1.9	100.0	44.7 $\pm$ 17.0	0.01 $\pm$ 0.02	0.980 $\pm$ 0.021	1.8
	Final Proj.	100.0	82.7 $\pm$ 15.9	0.15 $\pm$ 0.19	0.864 $\pm$ 0.065	5.8	100.0	94.3 $\pm$ 12.3	0.00 $\pm$ 0.01	0.953 $\pm$ 0.032	3.6	100.0	94.5 $\pm$ 12.5	0.00 $\pm$ 0.00	0.980 $\pm$ 0.019	5.2
	DiRecT (Ours)	100.0	96.6 $\pm$ 10.5	0.00 $\pm$ 0.00	0.835 $\pm$ 0.072	50.5	100.0	96.9 $\pm$ 10.3	0.00 $\pm$ 0.00	0.937 $\pm$ 0.043	27.7	100.0	96.9 $\pm$ 10.2	0.00 $\pm$ 0.00	0.981 $\pm$ 0.017	61.2
8	Diffuser	0.0	0.0 $\pm$ 0.0	41.62 $\pm$ 9.14	0.960 $\pm$ 0.025	1.2 $\pm$ 0.3	0.0	0.0 $\pm$ 0.0	41.62 $\pm$ 9.14	0.960 $\pm$ 0.025	1.2 $\pm$ 0.3	0.0	0.0 $\pm$ 0.0	41.62 $\pm$ 9.14	0.960 $\pm$ 0.025	1.2 $\pm$ 0.3
	MMD-CBS	100.0	100.0	0.00	-	22.3 $\pm$ 2.3	100.0	100.0	0.00	-	22.3 $\pm$ 2.3	100.0	100.0	0.00	-	22.3 $\pm$ 2.3
	PCD-LB	36.0	0.7 $\pm$ 1.4	7.87 $\pm$ 2.00	0.895 $\pm$ 0.052	2.4	48.0	1.1 $\pm$ 2.0	7.87 $\pm$ 1.94	0.969 $\pm$ 0.026	2.7	43.0	0.7 $\pm$ 1.2	8.32 $\pm$ 1.95	0.988 $\pm$ 0.014	2.3
	PCD-SHD	75.0	1.8 $\pm$ 2.7	0.39 $\pm$ 0.13	0.859 $\pm$ 0.050	2.4	89.0	3.8 $\pm$ 4.0	0.15 $\pm$ 0.06	0.940 $\pm$ 0.030	2.6	94.0	4.8 $\pm$ 4.2	0.04 $\pm$ 0.02	0.964 $\pm$ 0.018	2.3
	Final Proj.	100.0	50.8 $\pm$ 16.8	0.96 $\pm$ 0.70	0.845 $\pm$ 0.049	6.2	100.0	87.0 $\pm$ 16.5	0.02 $\pm$ 0.02	0.949 $\pm$ 0.023	4.2	100.0	88.5 $\pm$ 17.1	0.00 $\pm$ 0.01	0.976 $\pm$ 0.012	6.4
	DiRecT (Ours)	100.0	92.7 $\pm$ 13.4	0.01 $\pm$ 0.01	0.820 $\pm$ 0.053	66.0	100.0	93.9 $\pm$ 13.4	0.00 $\pm$ 0.00	0.933 $\pm$ 0.031	35.3	100.0	93.8 $\pm$ 13.5	0.00 $\pm$ 0.00	0.976 $\pm$ 0.013	67.7
12	Diffuser	0.0	0.0 $\pm$ 0.0	99.55 $\pm$ 11.98	0.961 $\pm$ 0.023	1.2 $\pm$ 0.4	0.0	0.0 $\pm$ 0.0	99.55 $\pm$ 11.98	0.961 $\pm$ 0.023	1.2 $\pm$ 0.4	0.0	0.0 $\pm$ 0.0	99.55 $\pm$ 11.98	0.961 $\pm$ 0.023	1.2

Table 10: MRMP results on Drop-Region. SR: success rate (%), CS: constraint safety (%), Coll: mean collisions, DA: data adherence, Time: computation time (s). Standard deviations are over different initializations and boldface represents best among the methods actively enforcing constraints.

# Ag.	Method	Low ( $v_{\max}=0.928$ )					Medium ( $v_{\max}=1.13$ )					High ( $v_{\max}=1.34$ )				
		SR $\uparrow$	CS $\uparrow$	Coll $\downarrow$	DA $\uparrow$	Time (s) $\downarrow$	SR $\uparrow$	CS $\uparrow$	Coll $\downarrow$	DA $\uparrow$	Time (s) $\downarrow$	SR $\uparrow$	CS $\uparrow$	Coll $\downarrow$	DA $\uparrow$	Time (s) $\downarrow$
4	Diffuser	40.0	1.1 $\pm$ 1.8	17.17 $\pm$ 3.75	0.991 $\pm$ 0.007	0.6 $\pm$ 0.4	40.0	1.1 $\pm$ 1.8	17.17 $\pm$ 3.75	0.991 $\pm$ 0.007	0.6 $\pm$ 0.4	40.0	1.1 $\pm$ 1.8	17.17 $\pm$ 3.75	0.991 $\pm$ 0.007	0.6 $\pm$ 0.4
	MMD-CBS	100.0	100.0	0.00	-	9.2 $\pm$ 1.0	100.0	100.0	0.00	-	9.2 $\pm$ 1.0	100.0	100.0	0.00	-	9.2 $\pm$ 1.0
	PCD-LB	<b>100.0</b>	38.6 $\pm$ 10.2	2.74 $\pm$ 0.85	<b>0.980</b> $\pm$ 0.017	1.9	<b>100.0</b>	36.6 $\pm$ 9.8	2.89 $\pm$ 0.86	<b>0.986</b> $\pm$ 0.013	1.9	<b>100.0</b>	36.1 $\pm$ 9.0	2.92 $\pm$ 0.80	<b>0.987</b> $\pm$ 0.010	1.8
	PCD-SHD	<b>100.0</b>	88.0 $\pm$ 6.2	0.05 $\pm$ 0.03	<b>0.965</b> $\pm$ 0.018	1.9	<b>100.0</b>	88.0 $\pm$ 5.1	0.04 $\pm$ 0.03	<b>0.965</b> $\pm$ 0.017	1.7	<b>100.0</b>	86.9 $\pm$ 5.2	0.02 $\pm$ 0.02	<b>0.965</b> $\pm$ 0.016	1.7
	Final Proj.	<b>100.0</b>	84.6 $\pm$ 11.9	0.35 $\pm$ 0.39	<b>0.980</b> $\pm$ 0.015	2.2	<b>100.0</b>	98.4 $\pm$ 2.1	0.03 $\pm$ 0.05	<b>0.989</b> $\pm$ 0.007	2.1	<b>100.0</b>	99.8 $\pm$ 0.5	<b>0.00</b> $\pm$ 0.01	<b>0.990</b> $\pm$ 0.007	5.9
	DiRecT (Ours)	<b>100.0</b>	<b>100.0</b> $\pm$ 0.0	<b>0.00</b> $\pm$ 0.00	<b>0.971</b> $\pm$ 0.021	25.4	<b>100.0</b>	<b>100.0</b> $\pm$ 0.0	<b>0.00</b> $\pm$ 0.00	<b>0.985</b> $\pm$ 0.011	24.2	<b>100.0</b>	<b>100.0</b> $\pm$ 0.0	<b>0.00</b> $\pm$ 0.00	<b>0.989</b> $\pm$ 0.008	65.0
8	Diffuser	0.0	0.0 $\pm$ 0.0	82.64 $\pm$ 9.51	0.991 $\pm$ 0.005	0.6 $\pm$ 0.4	0.0	0.0 $\pm$ 0.0	82.64 $\pm$ 9.51	0.991 $\pm$ 0.005	0.6 $\pm$ 0.4	0.0	0.0 $\pm$ 0.0	82.64 $\pm$ 9.51	0.991 $\pm$ 0.005	0.6 $\pm$ 0.4
	MMD-CBS	100.0	100.0	0.00	-	55.5 $\pm$ 1.9	100.0	100.0	0.00	-	55.5 $\pm$ 1.9	100.0	100.0	0.00	-	55.5 $\pm$ 1.9
	PCD-LB	11.0	0.1 $\pm$ 0.3	29.94 $\pm$ 3.91	<b>0.981</b> $\pm$ 0.014	3.5	7.0	0.1 $\pm$ 0.2	31.40 $\pm$ 3.80	<b>0.988</b> $\pm$ 0.009	2.3	2.0	0.0 $\pm$ 0.1	32.13 $\pm$ 3.91	<b>0.989</b> $\pm$ 0.008	2.1
	PCD-SHD	<b>100.0</b>	26.3 $\pm$ 7.1	0.45 $\pm$ 0.12	<b>0.883</b> $\pm$ 0.021	3.7	<b>100.0</b>	24.6 $\pm$ 6.5	0.34 $\pm$ 0.09	<b>0.883</b> $\pm$ 0.020	2.3	<b>100.0</b>	23.1 $\pm$ 6.1	0.18 $\pm$ 0.05	<b>0.880</b> $\pm$ 0.021	2.1
	Final Proj.	<b>100.0</b>	59.7 $\pm$ 16.6	1.76 $\pm$ 1.10	<b>0.971</b> $\pm$ 0.012	2.6	<b>100.0</b>	94.6 $\pm$ 4.1	0.14 $\pm$ 0.15	<b>0.983</b> $\pm$ 0.007	2.6	<b>100.0</b>	97.9 $\pm$ 1.5	0.02 $\pm$ 0.02	<b>0.985</b> $\pm$ 0.007	5.3
	DiRecT (Ours)	<b>100.0</b>	<b>100.0</b> $\pm$ 0.1	<b>0.00</b> $\pm$ 0.01	<b>0.965</b> $\pm$ 0.015	29.2	<b>100.0</b>	<b>100.0</b> $\pm$ 0.1	<b>0.00</b> $\pm$ 0.00	<b>0.982</b> $\pm$ 0.009	28.9	<b>100.0</b>	<b>100.0</b> $\pm$ 0.2	<b>0.00</b> $\pm$ 0.00	<b>0.986</b> $\pm$ 0.007	65.6
12	Diffuser	0.0	0.0 $\pm$ 0.0	194.40 $\pm$ 14.29	0.991 $\pm$ 0.004	0.7 $\pm$ 0.5	0.0	0.0 $\pm$ 0.0	194.40 $\pm$ 14.29	0.991 $\pm$ 0.004	0.7 $\pm$ 0.5	0.0	0.0 $\pm$ 0.0	194.40 $\pm$ 14.29	0.991 $\pm$ 0.004	0.7 $\pm$ 0.5
	MMD-CBS	0.0	8.3	12.00	-	67.8 $\pm$ 1.0	0.0	8.3	12.00	-	67.8 $\pm$ 1.0	0.0	8.3	12.00	-	67.8 $\pm$ 1.0
	PCD-LB	0.0	0.0 $\pm$ 0.0	94.96 $\pm$ 9.00	<b>0.982</b> $\pm$ 0.010	3.0	0.0	0.0 $\pm$ 0.0	98.91 $\pm$ 8.58	<b>0.989</b> $\pm$ 0.006	2.7	0.0	0.0 $\pm$ 0.0	100.86 $\pm$ 8.58	<b>0.990</b> $\pm$ 0.005	2.6
	PCD-SHD	71.0	1.1 $\pm$ 1.0	1.45 $\pm$ 0.19	<b>0.787</b> $\pm$ 0.025	4.5	60.0	0.8 $\pm$ 0.9	1.08 $\pm$ 0.18	<b>0.787</b> $\pm$ 0.023	2.8	50.0	0.6 $\pm$ 0.8	0.59 $\pm$ 0.09	<b>0.782</b> $\pm$ 0.023	2.7
	Final Proj.	<b>100.0</b>	33.4 $\pm$ 14.3	4.80 $\pm$ 2.24	<b>0.952</b> $\pm$ 0.012	4.1	<b>100.0</b>	83.6 $\pm$ 5.6	0.45 $\pm$ 0.28	<b>0.968</b> $\pm$ 0.008	4.1	<b>100.0</b>	89.6 $\pm$ 2.8	0.12 $\pm$ 0.04	<b>0.973</b> $\pm$ 0.007	8.2
	DiRecT (Ours)	<b>100.0</b>	<b>99.5</b> $\pm$ 0.1	<b>0.00</b> $\pm$ 0.01	<b>0.955</b> $\pm$ 0.016	47.7	<b>100.0</b>	<b>99.8</b> $\pm$ 0.3	<b>0.00</b> $\pm$ 0.01	<b>0.975</b> $\pm$ 0.008	47.4	<b>100.0</b>	<b>99.6</b> $\pm$ 0.6	<b>0.00</b> $\pm$ 0.01	<b>0.981</b> $\pm$ 0.006	67.0
16	Diffuser	0.0	0.0 $\pm$ 0.0	352.68 $\pm$ 19.38	0.991 $\pm$ 0.003	0.8 $\pm$ 0.5	0.0	0.0 $\pm$ 0.0	352.68 $\pm$ 19.38	0.991 $\pm$ 0.003	0.8 $\pm$ 0.5	0.0	0.0 $\pm$ 0.0	352.68 $\pm$ 19.38	0.991 $\pm$ 0.003	0.8 $\pm$ 0.5
	MMD-CBS	0.0	12.5	34.00	-	77.2 $\pm$ 3.7	0.0	12.5	34.00	-	77.2 $\pm$ 3.7	0.0	12.5	34.00	-	77.2 $\pm$ 3.7
	PCD-LB	0.0	0.0 $\pm$ 0.0	196.78 $\pm$ 13.86	<b>0.983</b> $\pm$ 0.008	4.1	0.0	0.0 $\pm$ 0.0	204.24 $\pm$ 12.63	<b>0.989</b> $\pm$ 0.005	3.5	0.0	0.0 $\pm$ 0.0	208.07 $\pm$ 12.00	<b>0.991</b> $\pm$ 0.004	3.3
	PCD-SHD	1.0	0.0 $\pm$ 0.1	3.12 $\pm$ 0.36	<b>0.710</b> $\pm$ 0.024	5.4	1.0	0.0 $\pm$ 0.1	2.24 $\pm$ 0.25	<b>0.709</b> $\pm$ 0.021	3.5	0.0	0.0 $\pm$ 0.0	1.27 $\pm$ 0.13	<b>0.703</b> $\pm$ 0.021	3.3
	Final Proj.	<b>100.0</b>	14.9 $\pm$ 8.8	9.88 $\pm$ 3.38	<b>0.919</b> $\pm$ 0.011	6.0	<b>100.0</b>	61.8 $\pm$ 7.4	1.25 $\pm$ 0.53	<b>0.940</b> $\pm$ 0.009	6.0	<b>100.0</b>	70.6 $\pm$ 5.3	0.42 $\pm$ 0.10	<b>0.950</b> $\pm$ 0.008	6.8
	DiRecT (Ours)	<b>100.0</b>	<b>99.5</b> $\pm$ 0.7	<b>0.01</b> $\pm$ 0.02	<b>0.938</b> $\pm$ 0.012	71.2	<b>100.0</b>	<b>99.1</b> $\pm$ 0.9	<b>0.01</b> $\pm$ 0.01	<b>0.961</b> $\pm$ 0.008	70.9	<b>100.0</b>	<b>98.4</b> $\pm$ 1.1	<b>0.02</b> $\pm$ 0.01	<b>0.971</b> $\pm$ 0.006	72.5
20	Diffuser	0.0	0.0 $\pm$ 0.0	568.27 $\pm$ 23.79	0.992 $\pm$ 0.003	1.0 $\pm$ 0.5	0.0	0.0 $\pm$ 0.0	568.27 $\pm$ 23.79	0.992 $\pm$ 0.003	1.0 $\pm$ 0.5	0.0	0.0 $\pm$ 0.0	568.27 $\pm$ 23.79	0.992 $\pm$ 0.003	1.0 $\pm$ 0.5
	MMD-CBS	0.0	0.0	48.00	-	99.0 $\pm$ 23.3	0.0	0.0	48.00	-	99.0 $\pm$ 23.3	0.0	0.0	48.00	-	99.0 $\pm$ 23.3
	PCD-LB	0.0	0.0 $\pm$ 0.0	342.21 $\pm$ 16.54	<b>0.982</b> $\pm$ 0.007	4.1	0.0	0.0 $\pm$ 0.0	355.78 $\pm$ 15.43	<b>0.989</b> $\pm$ 0.004	4.0	0.0	0.0 $\pm$ 0.0	361.93 $\pm$ 15.70	<b>0.990</b> $\pm$ 0.003	3.8
	PCD-SHD	0.0	0.0 $\pm$ 0.0	5.38 $\pm$ 0.59	<b>0.646</b> $\pm$ 0.015	6.7	0.0	0.0 $\pm$ 0.0	3.82 $\pm$ 0.35	<b>0.646</b> $\pm$ 0.015	4.0	0.0	0.0 $\pm$ 0.0	2.20 $\pm$ 0.20	<b>0.639</b> $\pm$ 0.014	3.8
	Final Proj.	88.0	3.1 $\pm$ 2.6	19.12 $\pm$ 4.73	<b>0.866</b> $\pm$ 0.017	8.4	<b>100.0</b>	32.1 $\pm$ 5.2	2.92 $\pm$ 0.69	<b>0.892</b> $\pm$ 0.014	8.3	<b>100.0</b>	42.0 $\pm$ 5.1	1.14 $\pm$ 0.18	<b>0.908</b> $\pm$ 0.013	8.4
	DiRecT (Ours)	<b>100.0</b>	<b>97.7</b> $\pm$ 1.3	<b>0.06</b> $\pm$ 0.04	<b>0.899</b> $\pm$ 0.018	100.5	<b>100.0</b>	<b>96.3</b> $\pm$ 1.6	<b>0.06</b> $\pm$ 0.03	<b>0.933</b> $\pm$ 0.010	99.7	<b>100.0</b>	<b>94.1</b> $\pm$ 2.4	<b>0.06</b> $\pm$ 0.03	<b>0.947</b> $\pm$ 0.009	103.5

#### E.4 Safe and diverse contact-rich manipulation

As outlined in the ablation studies of [43], task success and trajectory diversity (DTW, DFD) are conflicting objectives in the PushT task. Therefore, there exists a Pareto-optimality front that can be traced by varying coupling strength. We sweep the coupling strength coefficient for gradient guidance in PCD and the step size of the Projected Gradient Descent update  $\lambda_c$  for DiRecT. Figure 6 shows that Pareto fronts obtained with our method dominate those derived from PCD for both DPP and LB cost functions. Furthermore, DiRecT improves over the baselines while requiring only *half* the projection and gradient evaluations, as we start guidance in the second half of denoising. This highlights the importance of optimizing near the data distribution where constraints and costs are more naturally defined.

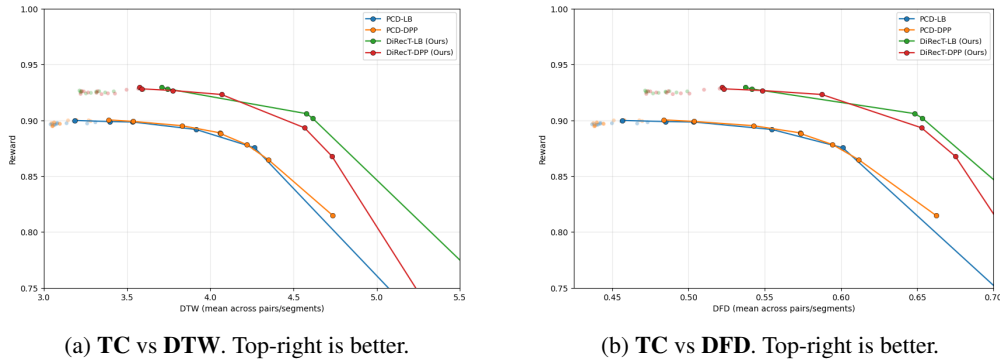


Figure 6: Pareto fronts for the PCD and DiRecT variants, obtained by sweeping the gradient coupling strength  $\gamma$  for PCD and the cost weight  $\lambda_c$  for DiRecT. Fronts are drawn as lines connecting Pareto-optimal points for each method, while dominated points are shaded.

## F Visualizations



Figure 7: Comparison of *planned* and *executed* trajectories for safe navigation in Maze2D-broad. Each row corresponds to a planning method.

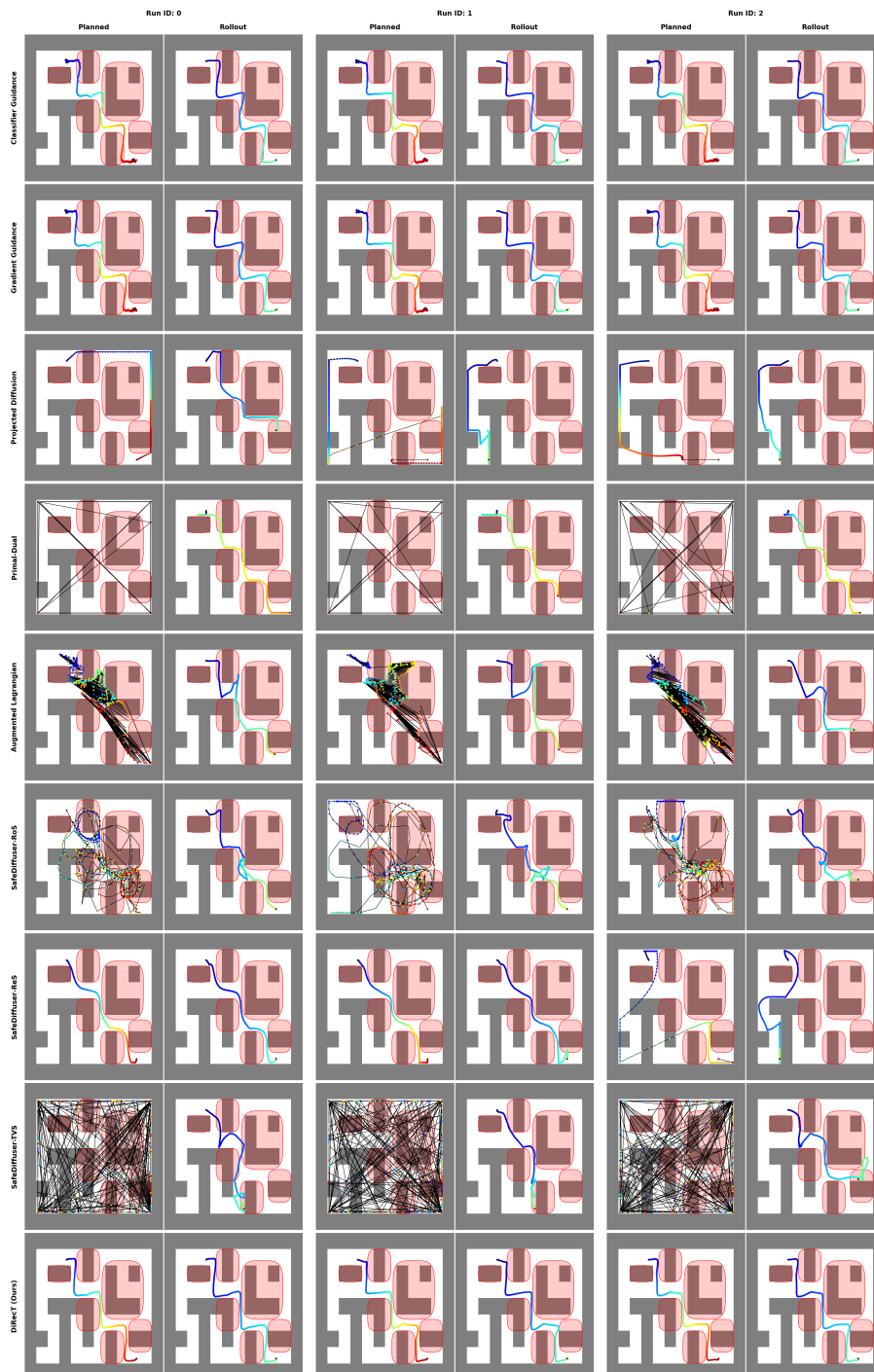


Figure 8: Comparison of *planned* and *executed* trajectories for safe navigation in Maze2D-narrow. Each row corresponds to a planning method.



Figure 9: Comparison of environment rollouts for different sampling schemes for safe manipulation in D3IL avoiding.

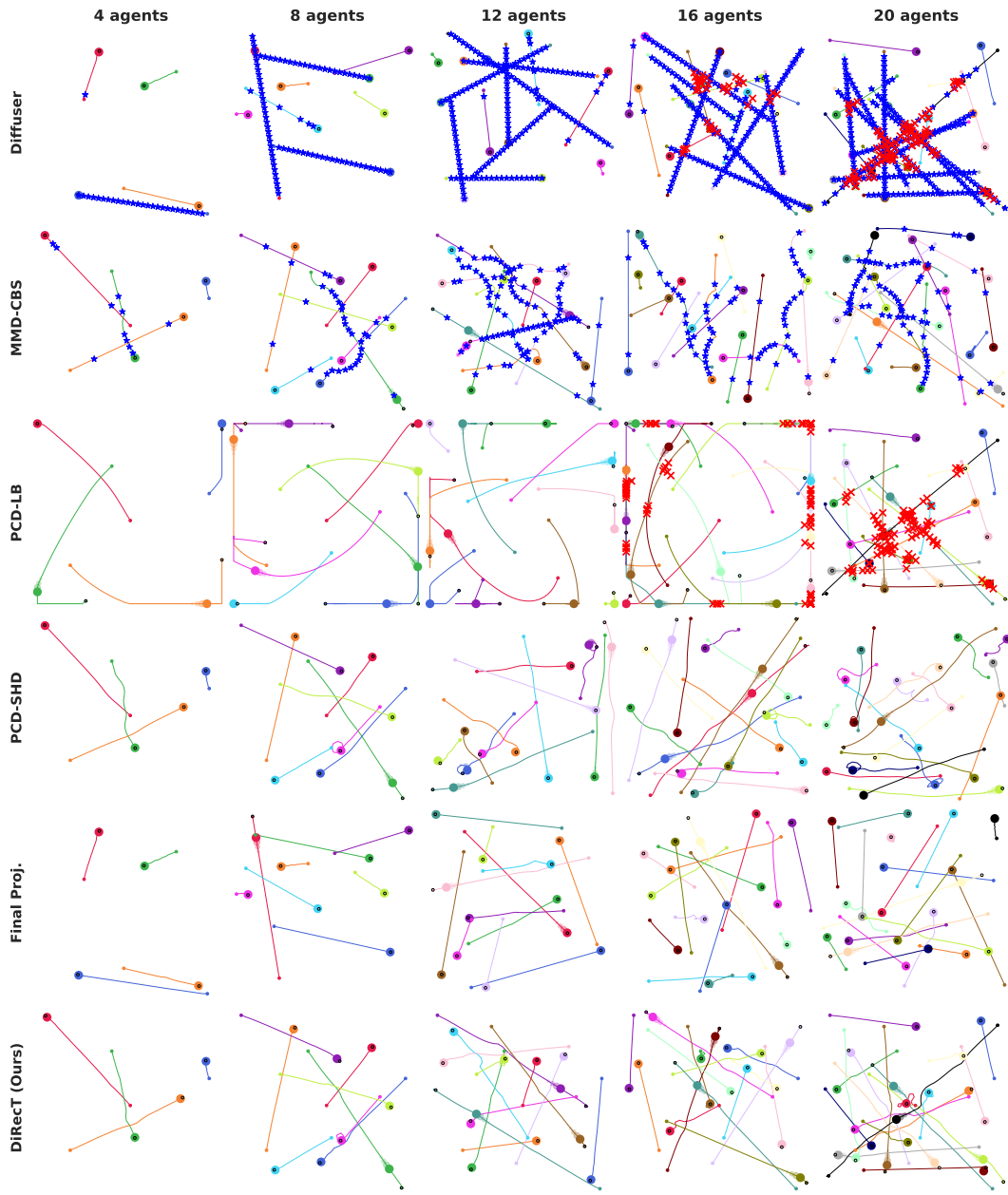


Figure 10: Visualizations of trajectories produced by different algorithms for the Empty MMD environment. Velocity is limited to 80% of the maximum action. Robots are rewarded for moving in a straight line, while avoiding collisions (red crosses) and velocity violations (blue stars).

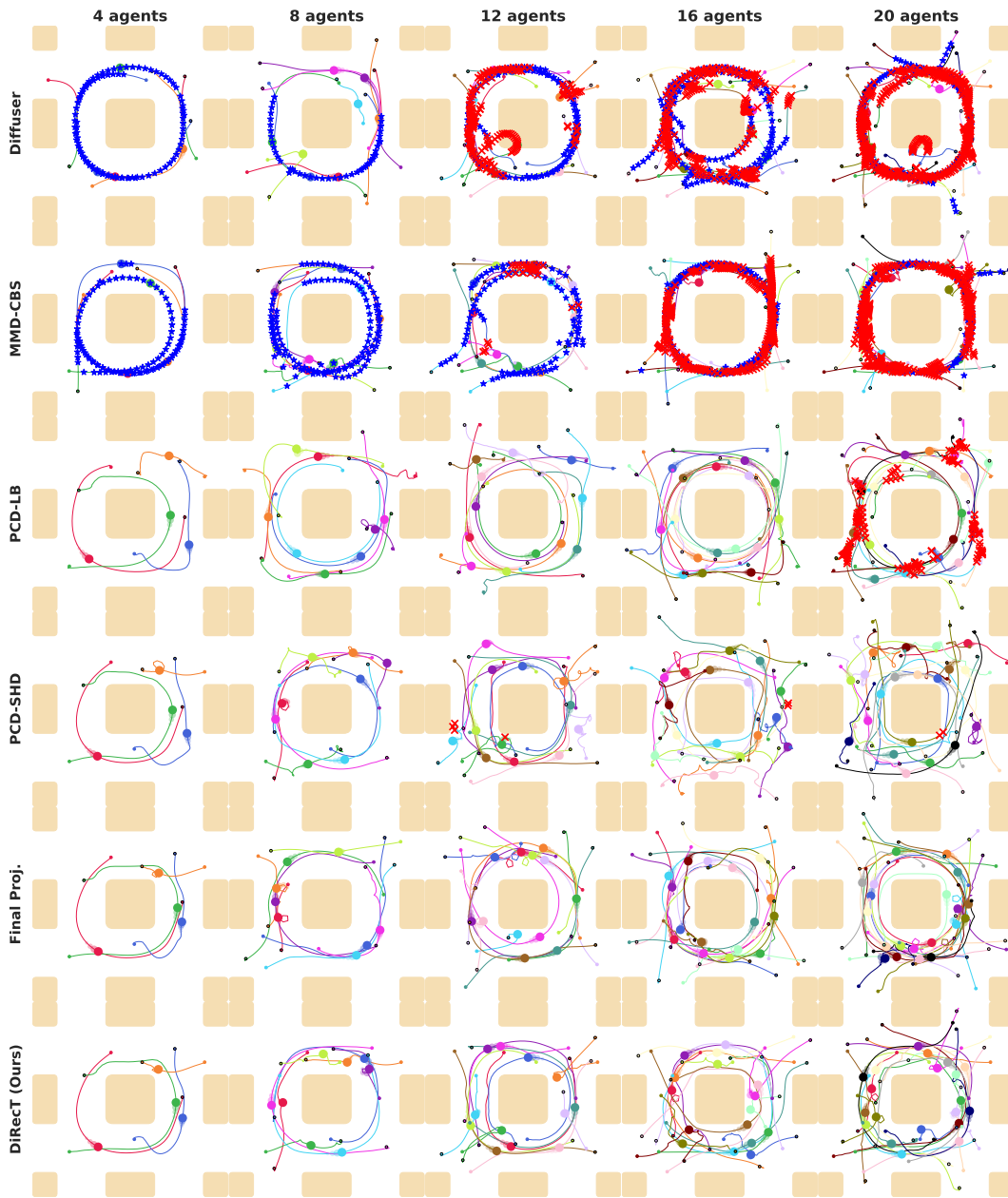


Figure 11: Visualizations of trajectories produced by different algorithms for the Highways MMD environment. Velocity is limited to 75% of the maximum action. Robots are rewarded for moving *counterclockwise* around the central obstacle, while avoiding collisions (red crosses) and velocity violations (blue stars).

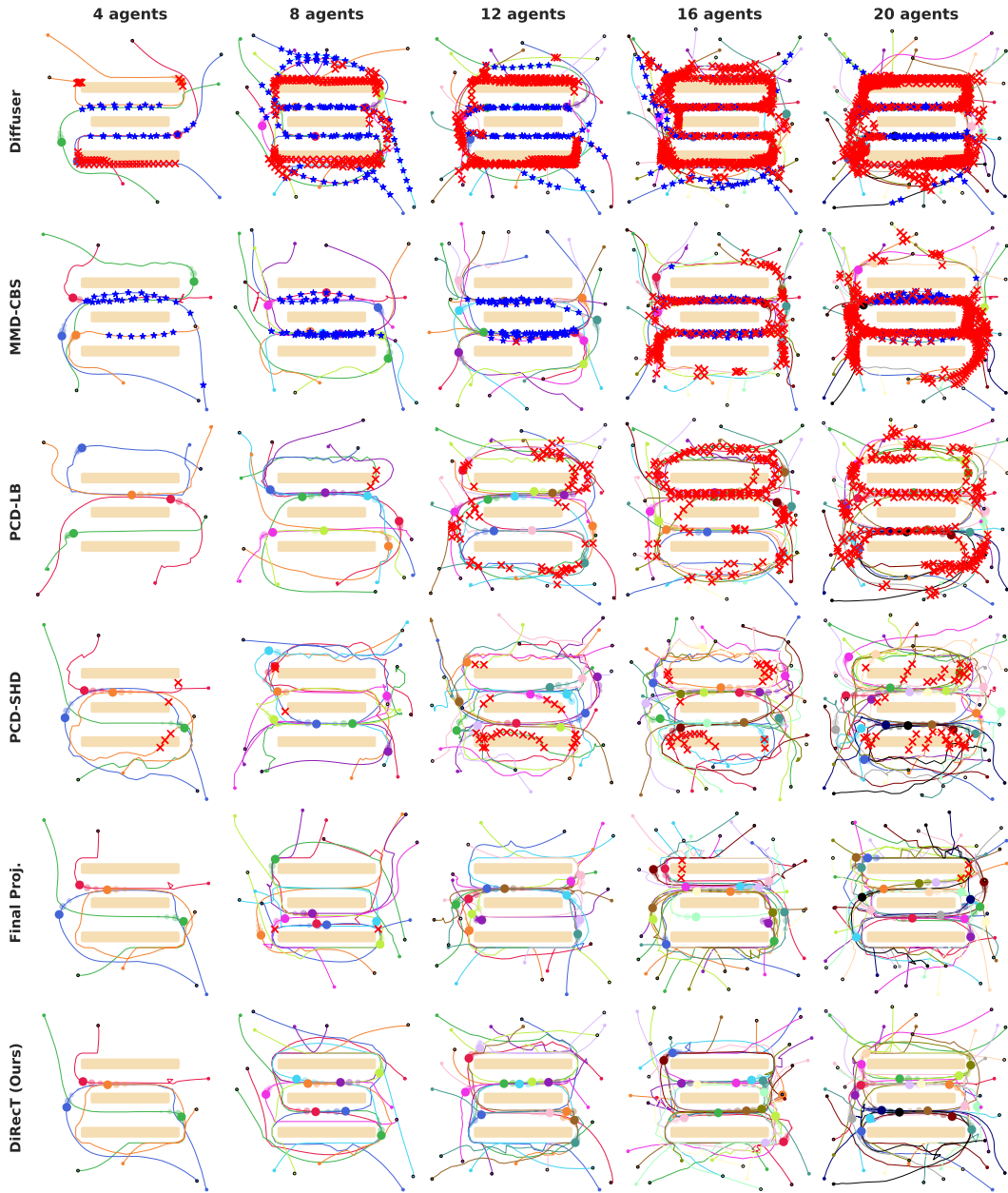


Figure 12: Visualizations of trajectories produced by different algorithms for the Conveyor MMD environment. Velocity is limited to 85% of the maximum action. Robots are rewarded for moving *leftward* in the top corridor and *rightward* in the bottom one, while avoiding collisions (red crosses) and velocity violations (blue stars).

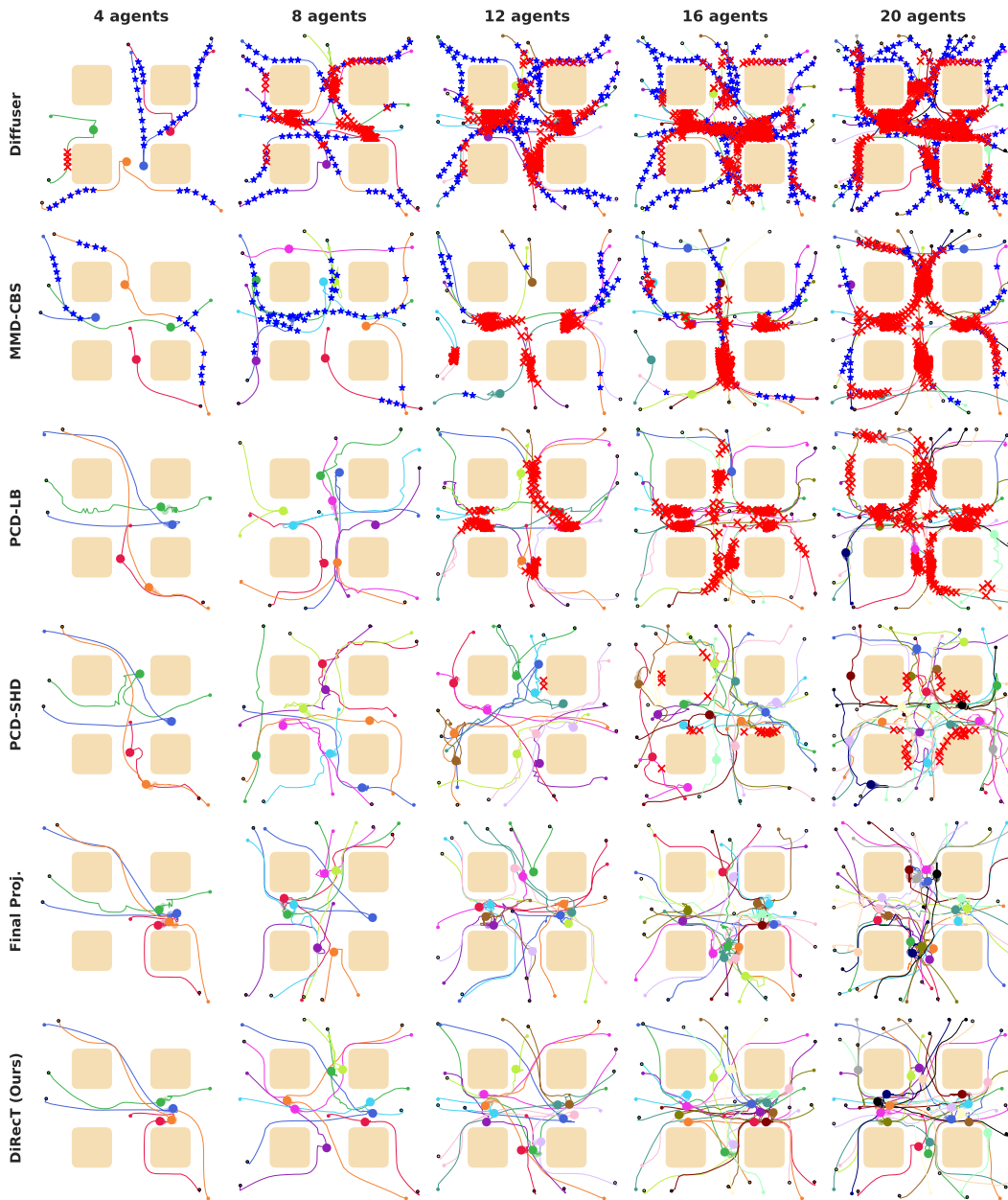


Figure 13: Visualizations of trajectories produced by different algorithms for the Drop-Region MMD environment. Velocity is limited to 85% of the maximum action. Robots are rewarded for *stopping* at the drop-off regions, while avoiding collisions (red crosses) and velocity violations (blue stars).



Figure 14: Visual comparison of different methods on coupled PushT generation with velocity constraints. Each column corresponds to the first sample of different initializations with red crosses to denote constraint violations. Only the first 64 executed steps are depicted to avoid clutter.